
STEIN DISCREPANCY FOR UNSUPERVISED DOMAIN ADAPTATION

A PREPRINT

Anneke von Seeger^{*1}, Dongmian Zou^{†2}, and Gilad Lerman^{‡1}

¹School of Mathematics, University of Minnesota, Minneapolis, MN, USA

²Data Science Research Center, Duke Kunshan University, Suzhou, Jiangsu, China

February 7, 2025

ABSTRACT

Unsupervised domain adaptation (UDA) leverages information from a labeled source dataset to improve accuracy on a related but unlabeled target dataset. A common approach to UDA is aligning representations from the source and target domains by minimizing the distance between their data distributions. Previous methods have employed distances such as Wasserstein distance and maximum mean discrepancy. However, these approaches are less effective when the target data is significantly scarcer than the source data. Stein discrepancy is an asymmetric distance between distributions that relies on one distribution only through its score function. In this paper, we propose a novel UDA method that uses Stein discrepancy to measure the distance between source and target domains. We develop a learning framework using both non-kernelized and kernelized Stein discrepancy. Theoretically, we derive an upper bound for the generalization error. Numerical experiments show that our method outperforms existing methods using other domain discrepancy measures when only small amounts of target data are available.

Keywords Machine Learning · Transfer Learning · Stein Discrepancy · Domain Adaptation

1 Introduction

Deep learning methods have been shown to outperform humans on tasks like image classification [He et al., 2015], but they typically require large amounts of labeled training data and assume that the training and test data are independent and identically distributed. In practice, both of these requirements can be difficult to satisfy. Unsupervised domain adaptation (UDA) addresses both of these challenges: it leverages information from a labeled source dataset to improve accuracy on a related but unlabeled target dataset [Ben-David et al., 2007, 2010]. Since unlabeled data is often easier and cheaper to obtain than labeled data, and relaxing the assumption that training and test data are identically distributed broadens the range of applicable datasets, UDA has become a crucial research area for solving real-world problems.

A common approach to UDA is feature alignment [Ganin and Lempitsky, 2015, Ganin et al., 2016, Long et al., 2015], whose goal is to learn feature representations that are informative for downstream tasks but invariant across domains. This can be accomplished by introducing a regularization term in the loss function that seeks to minimize the distance between the source and target feature distributions. Previous methods have used Wasserstein distance [Shen et al., 2018] and maximum mean discrepancy (MMD) [Long et al., 2017] to estimate the distance between distributions.

Existing UDA methods rely on a large, unlabeled target dataset to perform feature alignment. However, in some scenarios of interest, only a small amount of target data is available; we refer to this as the scarce target setting. For example, UDA has been applied to improve performance of machine learning models on electroencephalograms (EEGs), where patient-specific variations prevent directly transferring a model trained on one patient to new patients [Shi et al., 2024]. A UDA method that requires balanced sample sizes or abundant target data would be challenging to apply to a new patient, who might have only a small amount of data available. The scarce target setting also applies to online user

^{*}vonse006@umn.edu

[†]dongmian.zou@duke.edu

[‡]lerman@umn.edu

training, where a model, such as one trained to predict a search query from the first few words, might be trained on large amounts of data generated by many users and then fine-tuned to give personalized results using the much smaller amount of data associated with a single user.

Stein discrepancy [Stein, 1972] is a distance metric that performs well in the scarce target setting. Stein discrepancy is a distance metric well-suited for settings with limited samples. It measures the difference between distributions by applying a Stein operator \mathcal{A}_q to functions from a chosen function class \mathcal{F} , using the most discriminative function to compute the final discrepancy. For instance, kernelized Stein discrepancy (KSD) arises when \mathcal{F} is the unit ball of a reproducing kernel Hilbert space (RKHS), and provides a closed-form solution. The Stein discrepancy is closely related to integral probability metrics including the Wasserstein distance and MMD, which typically require integrating over both source and target distributions. However, a key advantage of Stein discrepancy is that it replaces the integration over the target distribution with a dependence on the score function through the Stein operator. In our method, this asymmetry allows us to estimate the Stein discrepancy even when the target domain contains significantly fewer samples than the source domain. On the other hand, it also necessitates special treatment of the target distribution, which we detail in our methodology. Additionally, the usage of Stein discrepancy is highly adaptable, and we derive multiple forms according to different assumptions of the target distribution.

We summarize our contributions as follows:

- We introduce a new UDA method based on Stein discrepancy, specifically designed for the scarce target setting, in which only a small amount of unlabeled target data is available.
- Our method is flexible: it has two forms, a non-kernelized form and a kernelized form, and several possible target distribution estimation approaches including a single Gaussian, GMM, or VAE.
- Our method can be integrated into various UDA frameworks, leveraging their respective advantages; here we integrate it with the JAN and SPA frameworks.
- We prove an upper bound on the target error that depends on the Stein discrepancy between the source and target distributions and the classification error on the source domain.
- Numerical experiments show that our method excels previous methods in the scarce target setting. Code is included in the supplemental information.

The rest of the paper is organized as follows: we begin with an overview of related works on domain adaptation and Stein discrepancy in Section 2. In Section 3, we review Stein discrepancy and KSD, introduce our method for UDA, and provide a generalization bound on the target error. Experimental results are introduced in Section 4, and the paper concludes in Section 5.

2 Related Works

We review related works in domain adaptation and Stein discrepancy, particularly the applications of the latter to machine learning and computational statistics. We refer the reader to [Liu et al., 2022] and [Anastasiou et al., 2023] for more comprehensive reviews of these topics.

2.1 Domain Adaptation

Foundational work for domain adaptation from Ben-David et al. [2007, 2010] proved an upper bound for the generalization error in the target domain that depends on the error in the source domain and the distance between the source and target distributions. This bound motivated a large class of domain adaptation methods focused on feature alignment, learning feature representations that are invariant between domains but informative for classification. The original bound used \mathcal{H} -divergence to measure the distance between domains, but \mathcal{H} -divergence is difficult to estimate in practice, so later algorithms used other distances between distributions, including Wasserstein distance [Courty et al., 2017], Jensen-Shannon divergence [Shui et al., 2022], α -Rényi distance [Mansour et al., 2009], and KL divergence [Nguyen et al., 2022]. MMD was used for several UDA methods [Long et al., 2015, 2017, Rozantsev et al., 2018], and is of particular interest because of connections between MMD and KSD. Several methods also took an adversarial approach to domain adaptation [Ganin and Lempitsky, 2015, Liu and Tuzel, 2016, Zhang et al., 2019], and they were later extended to conditional adversarial methods, inspired by conditional GANs [Long et al., 2018]. f-domain adversarial learning (FDAL) uses f-divergences to measure the distance between domains as part of an adversarial approach Acuna et al. [2021]. While adversarial methods are popular, challenges such as unstable training remain.

There exist other types of domain adaptation methods, which can often be paired with feature alignment methods to boost accuracy. Early but successful techniques included importance weighting, which emphasizes source samples that are similar to the target distribution [Gong et al., 2013, Long et al., 2014]. Another effective technique is pseudo-labeling

target samples before training a classifier on the target domain [Sohn et al., 2020]. Gradient harmonization, which seeks to resolve or reduce conflicts between the direction of the gradients from the two optimization goals, minimizing classification error and distance between domains, can boost performance by several percentage points on benchmark datasets [Huang et al., 2024]. Graph-based methods represent the source and target features as graphs and align the source and target domains by aligning characteristics of their graphs; graph spectral alignment (SPA) method attempts to align the graph spectra [Xiao et al., 2024].

There are several other common domain adaptation settings besides UDA. Semi-supervised domain adaptation has access to a small number of labels for the target distribution. Multi-source domain adaptation attempts to leverage information from several source domains at once, while multi-target attempts to improve performance over several target domains [Zhao et al., 2020]. Open set domain adaptation allows new classes in the target dataset that are not part of the source dataset [Panareda Busto and Gall, 2017]. Finally, domain generalization and few-shot learning are both similar to the scarce target setting for UDA. Domain generalization extends multi-source UDA by assuming that there is no access to the target data set; the goal is to learn features that are invariant to unseen distributions [Wang et al., 2022]. Domain generalization can be viewed as an extreme version of the scarce target setting, with no target data available, but does not leverage target information when it is available. Few-shot learning can refer to a broad class of methods focused on learning from few data points; however, unlike the scarce target setting, the data in few-shot learning is usually labeled [Parnami and Lee, 2022].

2.2 Stein Discrepancy

Stein’s method was introduced in 1972 to estimate distances between distributions [Stein, 1972], but it has gained popularity for applications in machine learning and computational statistics in the last decade because Stein discrepancies can be calculated for unnormalized distributions. Computing a Stein discrepancy usually involves a maximization, but most applications have focused on computable Stein discrepancies, which have a closed-form solution. Stein discrepancies were used to estimate sample quality, motivated by development of approximate MCMC schemes, which increase the speed of sampling at the cost of introducing bias [Gorham and Mackey, 2015, 2017]. Liu et al. [2016] and Chwialkowski et al. [2016] simultaneously developed KSD, a closed form solution to Stein discrepancy over an RKHS. Gorham and Mackey [2017] developed theory on when convergence in KSD will guarantee weak convergence between distributions, and demonstrated that in dimensions $d \geq 3$, commonly used kernels such as Gaussian and Matérn kernels fail to detect when a sample is not converging to a target. Stein discrepancies were also used to construct sample approximations, through Stein Variational Gradient Descent (SVGD) [Liu and Wang, 2019], which iteratively updates the location of samples; Stein points [Chen et al., 2018], which constructs a sample by sequentially adding points; and Stein thinning [Riabiz et al., 2022], which compresses an existing sample approximation, all with the goal of minimizing KSD. Finally, KSD was extended to a non-parametric form, in which the score function of an implicit model is estimated, and applied to two-sample tests for samples generated by implicit generative models. Two-sample tests for implicit generative models must be able to handle unbalanced sample sizes, since models can generate unlimited synthetic data while real data remains limited [Xu and Reinert, 2022]. This imbalance is analogous to our scarce target setting, where target domain samples are also limited compared to source domain.

3 Stein Discrepancy for Domain Adaptation

We begin with an overview of Stein discrepancies and KSD, before describing how to apply it to domain adaptation and providing an error bound.

3.1 Preliminaries

The starting point for Stein discrepancy is Stein’s identity for a distribution q and a Stein operator \mathcal{A}_q . This operator \mathcal{A}_q acts on functions from an associated set \mathcal{F} , known as the Stein class. Stein’s identity holds for any function $f \in \mathcal{F}$: $\mathbb{E}_{x \sim q}[\mathcal{A}_q f(x)] = 0$. We will focus on the score-Stein operator:

$$\mathcal{A}_q f(x) = f(x)^\top \nabla_x \log q(x) + \nabla_x \cdot f(x),$$

also called the Langevin Stein operator [Anastasiou et al., 2023]. The corresponding Stein class \mathcal{F} contains functions that satisfy $\lim_{\|x\| \rightarrow \infty} f(x)^\top \nabla_x \log q(x) = 0$, a relatively mild condition that includes all distributions with compact support. If the expectation over q in Stein’s identity is replaced by expectation over another smooth distribution p , then a simple calculation shows

$$\mathbb{E}_{x \sim p}[\mathcal{A}_q f] = \mathbb{E}_{x \sim p}[f(x) (\nabla_x \log p(x) - \nabla_x \log q(x))].$$

Finding the most discriminant $f \in \mathcal{F}$ gives a measure of the distance between p and q .

Definition 3.1 (Stein discrepancy). For smooth distributions p and q , the Stein discrepancy is defined as

$$S(p, q) = \sup_{f \in \mathcal{F}} \mathbb{E}_{x \sim p}[\mathcal{A}_q f(x)]. \quad (1)$$

The choice of the function class \mathcal{F} is crucial: \mathcal{F} should be large enough to detect differences between any two distributions of interest, while being simple enough that identifying the most discriminant $f \in \mathcal{F}$ is tractable. When \mathcal{F} is the unit ball of an RKHS, the optimization has a closed form solution [Chwialkowski et al., 2016, Liu et al., 2016]. An RKHS is a Hilbert space \mathcal{H} associated with a reproducing kernel, $k(\cdot, \cdot)$, which is positive definite and satisfy the reproducing property: $f(x) = \langle f(\cdot), k(x, \cdot) \rangle_{\mathcal{H}}$, for any $f \in \mathcal{F}$. A common choice of kernel is the radial basis function (RBF) kernel: $k(x, x') = \exp(-\|x - x'\|^2 / (2\sigma^2))$, where σ is the bandwidth. Due to the reproducing property of the kernel, $\mathbb{E}_{x \sim p}[\mathcal{A}_q f(x)]$ can be rewritten as an inner product:

$$\mathbb{E}_{x \sim p}[\mathcal{A}_q f(x)] = \langle f(\cdot), \mathbb{E}_{x \sim p}[\mathcal{A}_q k(x, \cdot)] \rangle_{\mathcal{H}}.$$

Maximizing over an inner product is straightforward. The closed form solution is called the kernelized Stein discrepancy (KSD):

$$S(p, q) = \mathbb{E}_{x, x' \sim p}[\mathcal{A}_q \mathcal{A}_q k(x, x')]. \quad (2)$$

Given an independent, identically distributed sample $\{x_i\}_{i=1}^n$ and a score function for q , denoted $s_q(x)$, KSD can be estimated by a U-statistic:

$$\hat{S}(p, q) = \frac{1}{n(n-1)} \sum_{1 \leq i \neq j \leq n} u_q(x_i, x_j),$$

where

$$u_q(x, x') = s_q(x)^\top k(x, x') s_q(x') + s_q(x)^\top \nabla_{x'} k(x, x') + \nabla_x k(x, x')^\top s_q(x') + \text{trace}(\nabla_{x, x'} k(x, x')).$$

This U-statistic provides a minimum-variance, unbiased estimate of $S(p, q)$. If $p \neq q$, then $\hat{S}(p, q)$ converges to $S(p, q)$ with rate $O(n^{-1})$, where n is the number of samples from the source distribution. If $p = q$, then $\hat{S}(p, q)$ converges with rate $O(n^{-1/2})$ [Liu et al., 2016]. The convergence rate with respect to the number of target samples depends on the choice of model for the target distribution; if the target distribution is modeled by a Gaussian, it converges with rate $O(m^{-1/2})$, where m is the number of target samples.

Stein discrepancy is closely related to integral probability metrics (IPMs). IPMs include many probability metrics of interest, several of which have been applied to previous UDA methods, and can be written as

$$d_{\mathcal{F}}(p, q) = \sup_{f \in \mathcal{F}} \mathbb{E}_p[f(x)] - \mathbb{E}_q[f(x)].$$

For instance, if \mathcal{F} is the set of 1-Lipschitz functions, $d_{\mathcal{F}}(p, q)$ is the 1-Wasserstein distance between the distributions. If \mathcal{F} is the unit ball of an RKHS, then $d_{\mathcal{F}}(p, q)$ is the MMD. An IPM can be rewritten as a Stein discrepancy for test functions h that solve the Stein equation: $\mathcal{A}_q f(x) = h(x) - \mathbb{E}_q[h(x)]$, and a solution is guaranteed to exist for many settings of interest [Anastasiou et al., 2023]. The advantage in rewriting an IPM as a Stein discrepancy is that instead of taking an expectation over both distributions, as required to calculate an IPM, calculating a Stein discrepancy only requires an expectation over one distribution; the second distribution influences the Stein discrepancy only through its score function. Another way of viewing this advantage is that more randomness enters $S(p, q)$ through the samples from p than from q . The consequence is that we can accurately estimate $S(p, q)$ with small amounts of data from q .

3.2 Methodology

To apply Stein discrepancy to domain adaptation, let x_S, x_T denote samples drawn from the source and target distributions $\mathcal{D}_S, \mathcal{D}_T$ respectively. Since this method is focused on UDA, source labels y_S are available but no target labels y_T are available.

A common framework in domain adaptation, which we adopt here, is feature alignment, where the goal is to learn features that are informative for classification but invariant between domains. To accomplish this, features $z = g(x)$ are extracted by a function g , which is identical in both source and target domains. Training seeks to simultaneously minimize the transfer loss \mathcal{L}_D , which measures the distance between the source and target domains, and the classification loss on the source domain \mathcal{L}_C . Any standard classification loss can be used, such as cross-entropy loss. Our method uses Stein discrepancy as the transfer loss and we derive two forms: an adversarial form, based on (1):

$$\mathcal{L}_D(\mathcal{D}_S, \mathcal{D}_T) = \sup_{f \in \mathcal{F}} \mathbb{E}_{\mathcal{D}_S}[\mathcal{A}_{\mathcal{D}_T} f(x)]$$

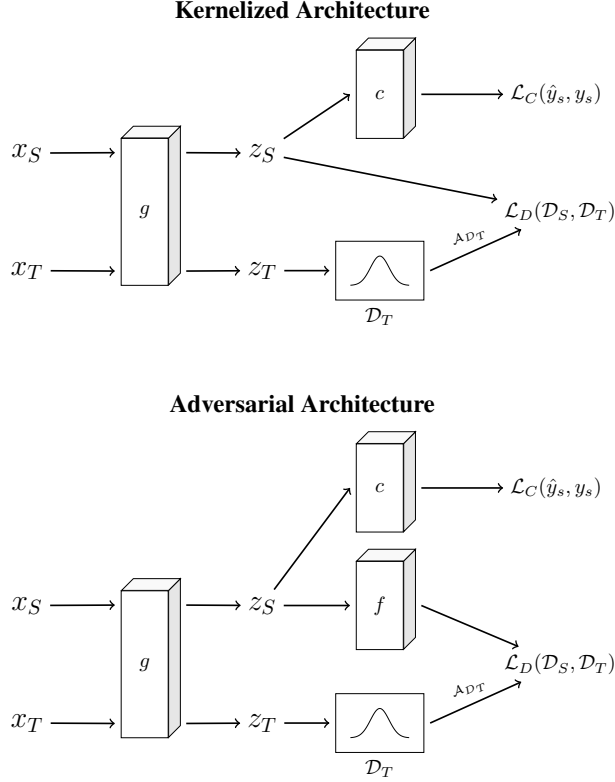


Figure 1: Architecture for Stein discrepancy-based UDA. Source and target data, x_S, x_T pass through a feature extractor g . Source features z_S classified by c and classification loss \mathcal{L}_C is calculated. Target features z_T are used to estimate a target distribution; the score function is $\nabla \log \mathcal{D}_T$ is used in the Stein operator $\mathcal{A}_{\mathcal{D}_T}$. Top (kernelized architecture): \mathcal{L}_D is defined according to (2): $\mathcal{L}_D = \mathbb{E}_{z_S} [\mathcal{A}_{\mathcal{D}_T} \mathcal{A}_{\mathcal{D}_T} k(z_S, z'_S)]$. Training minimizes $\mathcal{L}_C + \lambda \mathcal{L}_D$ over g, c , where λ is a trade-off parameter between the two losses. Bottom (adversarial architecture): \mathcal{L}_D is defined according to (1): $\mathcal{L}_D = \max_{f \in \mathcal{F}} \mathbb{E}_{z_S} [\mathcal{A}_{\mathcal{D}_T} f(z_S)]$. Training maximizes over f to estimate \mathcal{L}_D and minimizes $\mathcal{L}_C + \lambda \mathcal{L}_D$ over g, c .

and a kernelized form, based on (2):

$$\mathcal{L}_D(\mathcal{D}_S, \mathcal{D}_T) = \mathbb{E}_{x, x' \sim \mathcal{D}_S} [\mathcal{A}_{\mathcal{D}_T} \mathcal{A}_{\mathcal{D}_T} k(x, x')].$$

Training the adversarial form requires a min-max optimization because estimating $\mathcal{L}_D(\mathcal{D}_S, \mathcal{D}_T)$ requires maximizing to find the most discriminant f . Given an estimate of $\mathcal{L}_D(\mathcal{D}_S, \mathcal{D}_T)$, $\mathcal{L}_D(\mathcal{D}_S, \mathcal{D}_T)$ and \mathcal{L}_C are both minimized. Training the kernelized form requires only minimization. The architecture for both forms is shown in Figure 1.

The asymmetry in Stein discrepancy gives an advantage in the scarce target setting to Stein discrepancy-based methods over domain adaptation methods based on traditional IPMs, such as Wasserstein distance and MMD [Courty et al., 2017, Long et al., 2015, 2017]. Since the expectation is taken only over \mathcal{D}_S , and \mathcal{D}_T only appears via its score function, randomness enters $\mathcal{L}_D(\mathcal{D}_S, \mathcal{D}_T)$ mainly through the samples $x, x' \sim \mathcal{D}_S$, and $\mathcal{L}_D(\mathcal{D}_S, \mathcal{D}_T)$ can be accurately estimated even when only a small amount of target data is available.

Estimating the Stein discrepancy requires a score function for \mathcal{D}_T to be expressed in a parametric form. This parametric form must be simple enough to admit an explicit and tractable computation of the score function, while being flexible enough to describe complex distributions from real data. We propose three possible models for the target distribution: a Gaussian model, a Gaussian mixture model (GMM), and a variational autoencoder (VAE).

Gaussian. A Gaussian distribution $\mathcal{N}(\mu, \Sigma)$ with mean μ and covariance Σ has a simple score function:

$$\nabla \log \mathcal{D}_T(z) = -\Sigma^{-1}(z - \mu). \quad (3)$$

In our method, we estimate the parameters using the sample mean and sample covariance from the data.

GMM. A GMM, a weighted sum of k Gaussians with weights $\{w_i\}_{i=1}^k$ where $\sum_{i=1}^k w_i = 1$, has a score function that is closely related to the Gaussian score function:

$$\nabla \log \mathcal{D}_T(z) = - \sum_{i=1}^k \gamma_i(z) \Sigma_i^{-1} (z - \mu_i), \quad (4)$$

where

$$\gamma_i(z) = \frac{w_i \mathcal{N}(z | \mu_i, \Sigma_i)}{\sum_{j=1}^k w_j \mathcal{N}(z | \mu_j, \Sigma_j)}.$$

In our method, the weights and parameters of Gaussians can be estimated using the EM algorithm.

VAE. A VAE, which is made up of an encoder and a decoder, embeds the data in a latent space, which is usually of lower dimension and is assumed to have a simple prior distribution, often a normal distribution. Passing a sample from the latent space through the decoder should generate a sample from the original, more complex distribution [Luo, 2022]. Letting \mathbf{E} denote the encoder, \mathbf{D} denote the decoder, ξ denote samples in the latent space, $p(z|\xi)$, $q(\xi|z)$ denote the conditional distributions in the original and latent space respectively, and assuming $\xi \sim \mathcal{N}(\mu, \Sigma)$, the score function is:

$$\nabla_z \log p(z) = \mathbb{E}_{q(\xi|z)} [\nabla_z p(z|\xi) p(z|\xi)], \quad (5)$$

where

$$\begin{aligned} & \nabla_z p(z|\xi) p(z|\xi) \\ &= \left[\frac{1}{(2\pi)^{d/2}} \exp \left(-\frac{\|z - \mathbf{D}(\xi)\|^2}{2} \right) \right]^2 (\mathbf{D}(\xi) - z). \end{aligned}$$

The derivation of (5) is included in Appendix C. The parameters of the VAE are trained together with other parameters in our model.

There is a tradeoff when selecting between the three models. The Gaussian model is straightforward to calculate and has the smallest number of parameters, but cannot accurately model complex data distributions. Using a VAE to model the target distribution is the most flexible choice for complex data distributions, but adds additional training time and instability, as it can be challenging to train the VAE to model the target distribution, while training is simultaneously updating the feature distribution to align source and target features. In numerical results, the GMM gave the best balance between a more flexible distribution and a more stable training process.

3.3 Bounds on Target Error

We prove a generalization bound on the target error, making use of theoretical framework developed for domain adaptation [Ben-David et al., 2007, 2010, Long et al., 2015] and Stein discrepancies [Anastasiou et al., 2023, Liu et al., 2016]. The proof can be found in Appendix A.

Theorem 3.2. *Let $\mathcal{D}_S, \mathcal{D}_T$ be probability distributions on the feature space X and \mathcal{F} be the unit ball of an RKHS with kernel $k(x, x')$, with $x, x' \in X$. Let f_S^* and f_T^* denote the true labeling functions associated with the source and target distributions, respectively. Let $\epsilon_T(f) = \mathbb{E}_{x \sim \mathcal{D}_T} [|f(x) - f_T^*(x)|]$ be the error function in the target domain, and $\epsilon_S(f)$ defined similarly for the source domain. Then the following bound holds for any labeling function $f \in \mathcal{F}$:*

$$\epsilon_T(f) \leq \epsilon_S(f) + 2\sqrt{S(\mathcal{D}_S, \mathcal{D}_T)} + C, \quad (6)$$

where $S(\cdot, \cdot)$ is the Stein discrepancy, and C depends on \mathcal{F} and sample size.

Theorem 3.2 suggests that in addition to minimizing the error in the source domain, minimizing the KSD leads to minimizing the target error. The proof relies on a connection between KSD and MMD [Liu et al., 2016]. While this property has been shown for other discrepancies, in particular MMD, the main advantage of the Stein discrepancy has been noticed in practice. Specifically, it has an advantage in the scarce target setting, with small amounts of target data and larger amounts of source data, which leads to unbalanced sample sizes. MMD has a high error rate in this case; numerical experiments from Xu and Reinert [2022] show that the type I error rate in two-sample testing for MMD can be as high as 100% with samples of sizes 50 and 1000. On the other hand, Xu and Reinert [2022] show that KSD is not negatively impacted by unbalanced sample sizes to the same extent and maintains an error rate under 10% in the same setting. We hypothesize that this is due to the replacement of the expectation over \mathcal{D}_T in MMD by the score function $\nabla_x \log \mathcal{D}_T(x)$ in KSD. For small sample sizes, estimating either the score function or the expectation of an unknown distribution may have significant error, and asymptotic rates of convergence to the true score function or the true expectation are not applicable when only a few dozen samples are available. However, estimating the score function under the assumption of a particular distribution, such as Gaussian, will provide information about the

whole distribution, unlike the numerical integration in the expectation, which will only provide information about the range in which samples are available. Assuming a large number of samples from the target distribution, information about a wider range of the distribution from the score function will provide a better alignment between the source and target distributions than an alignment that relies on the expectation. The main concern then is whether the choice of distribution is a good model for the true data distribution; a bad choice of target distribution could introduce significant bias into the model. In the absence of information about the true distribution, the simplest model (i.e. Gaussian) is usually best. Our numerical results also assess the impact of choosing more complex, flexible distributions, such as GMM or VAE.

4 Experiments

We evaluate the proposed method against baseline UDA methods. Code for our implementation is available in the supplemental material.

4.1 Setup

We use several standard datasets for UDA benchmarks, including Office31 [Saenko et al., 2010], Office-Home [Venkateswara et al., 2017], and VisDA-2017 [Peng et al., 2017]. Office31 contains 4,652 images from 31 classes of common office items, with three domains: Amazon (A), webcam (W), and DSLR (D). Office-Home contains approximately 15,500 images across 65 categories, with four domains: Art (Ar), Clipart (Cl), Product (Pr), and Real-world (Rw). VisDA-2017 contains over 280,000 images across 12 categories and contains two domains, synthetic (S) and real (R). Office31 and Office-Home are evaluated on all domain-pairs; VisDA-2017 is only evaluated on transfer from synthetic images to real images. To simulate the scarce target data setting, we use only 32 samples from the target data in Office31. We use a minimum of 1% of the target data or 32 samples from Office-Home. For VisDA-2017, which is the largest dataset with approximately 55,000 images in the target domain, we consider both scenarios maintaining 1% and 0.1% of the target data to ensure that the setting is truly scarce, since 1% of the data may have too many samples.

We compare our method against Deep Adversarial Neural Network (DANN) [Ganin and Lempitsky, 2015], Deep Adaptation Network (DAN) [Long et al., 2015], Joint Adaptation Network (JAN) [Long et al., 2017], Adversarial Discriminative Domain Adaptation (ADDA) [Tzeng et al., 2017], Conditional Domain Adversarial Network (CDAN) [Long et al., 2018], Batch Spectral Penalization (BSP) [Chen et al., 2019], Adaptive Feature Norm (AFN) [Xu et al., 2019], Maximum Classifier Discrepancy (MCD) [Saito et al., 2018], Margin Disparity Discrepancy (MDD) [Zhang et al., 2019], and Minimum Class Confusion (MCC) [Jin et al., 2020], f-Domain Adversarial Learning (FDAL) [Acuna et al., 2021], and Graph SPectral Alignment (SPA) [Xiao et al., 2024]. We also include Empirical Risk Minimization (ERM), a model trained only on source data and evaluated on target data, as a baseline. The baseline methods, except for FDAL and SPA, were implemented using the Transfer Learning Library (TLL) [Jiang et al., 2020, 2022]. FDAL and SPA were implemented following the code made available in the original papers.

We follow the same framework for implementation as in TLL, including identical data preprocessing and augmentation, to ensure comparable results. We use ResNet-50 [He et al., 2016] as the feature extractor on the Office31 and Office-Home datasets and ResNet-101 on VisDA-2017; the features are classified using a single-layer fully connected neural network. For the adversarial methods, the discriminator f is implemented as a fully-connected neural network with one layer for a Gaussian target distribution and two layers for a GMM or VAE target distribution. An RBF kernel is used for the kernelized methods, and the code to calculate KSD is adapted from [Korba et al., 2021].

Finally, we present both a standard implementation of our approach and an implementation that adapts SPA. The architecture of the standard implementation closely follows that of JAN, which is an MMD-based method. SPA incorporates two components based on graphs of images into the loss function, in addition to classification loss and a measure of distance between domains; we adapted SPA by replacing the domain distance, which used DANN or CDAN in the original implementation, with Stein discrepancy. The SPA-based implementation serves as a proof of concept to incorporate recent advancements UDA and to evaluate whether Stein discrepancy retains its advantage in light of these developments. Results should be assumed to be from the standard implementation, unless they are labeled as coming from the SPA framework.

Hyperparameters were selected using the HyperOpt search algorithm [Bergstra et al., 2013], implemented in Raytune [Liaw et al., 2018]; best hyperparameters on VisDA2017 are reported in Appendix E. For other methods, we keep the hyperparameters at the default value from TLL or from the original implementations. All the experiments are implemented on a server with A100 GPUs.

4.2 Results

For all methods, we report the average accuracy of the three highest-performing model runs in the scarce target setting on each domain, and report the pooled standard deviation. Results for the full target setting and for each domain are reported individually in Appendix B. Experimental results on Office31, Office-Home and VisDA-2017 are reported in Figures 2–4, respectively.

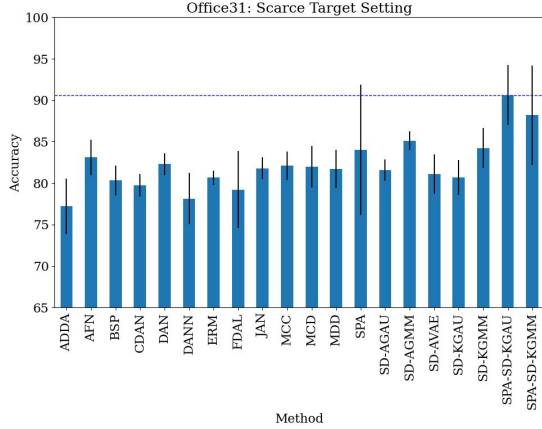


Figure 2: Average accuracy across 6 domain pairs (with pooled standard deviation) on Office31 dataset in scarce target setting (32 samples from target data). Horizontal line denotes the highest accuracy. The rightmost seven results correspond to our Stein discrepancy-based method.

We report accuracy for seven Stein discrepancy-based methods at the right of each figure, including five methods that follow the framework from JAN and two that use the SPA framework. The AGAU, AGMM, and AVAE methods use the adversarial loss function, with Gaussian, GMM, and VAE models for the target distribution respectively. The KGAU and KGMM methods use the kernelized loss function, with Gaussian and GMM target distributions. The kernelized method failed to sufficiently learn the target distribution with a VAE and the accuracy was much worse than other methods.

Across all three benchmark datasets, Stein discrepancy-based methods outperform comparable methods in the scarce target setting; in particular the standard implementation of Stein discrepancy methods framework outperform all but the SPA methods, and Stein discrepancy-based SPA methods outperform traditional SPA. This suggests that Stein discrepancy can be combined with other UDA methods to provide an advantage in the scarce target setting, while benefiting from the advantages of the method it is being combined with. On each dataset, the Stein discrepancy-based methods with SPA framework are the highest performing methods, with SPA-SD-KGAU achieving 90% accuracy on Office31 and both target distributions achieving 72% accuracy on Office-Home. On VisDA2017, SPA is the best-performing method in the 1% setting, achieving 78% accuracy. This suggests that 1% of the target data from VisDA2017 (550 samples) may be abundant enough that the Stein discrepancy gives limited advantage and other methods can perform well, although SPA-SD-KGAU is competitive with original SPA in this setting. However, in the 0.1% setting, the Stein discrepancy-based methods outperform SPA, with SPA-SD-KGAU achieving 74% accuracy. A significant drawback shared by

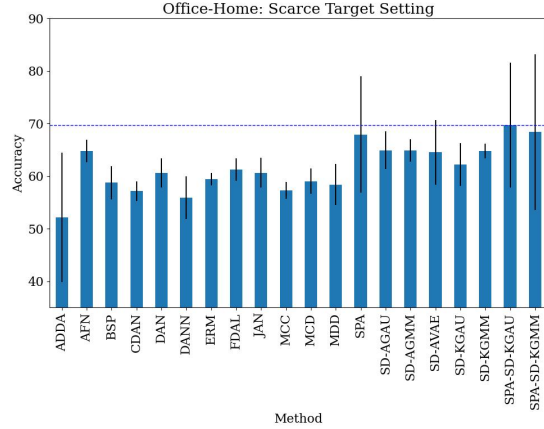


Figure 3: Average accuracy across 12 domain pairs (with pooled standard deviation) on Office-Home dataset in scarce target setting (minimum of 1% of target data or 32 samples). Horizontal line denotes the highest accuracy. The rightmost seven results correspond to our Stein discrepancy-based method.

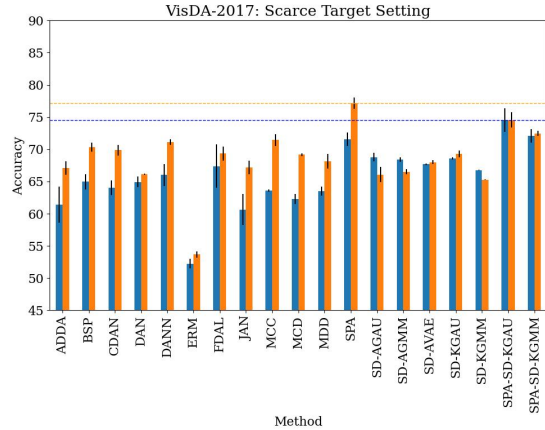


Figure 4: Accuracy and standard deviation on VisDA-2017 dataset, with 1% (orange) and 0.1% (blue) of target data available during training. Horizontal lines denote the highest accuracy. The rightmost seven results correspond to our Stein discrepancy-based method.

all of the SPA methods is the high variance in the scarce target setting, notably much higher variance than the Stein discrepancy-based methods with JAN framework. This may suggest the need to continue evaluating frameworks beyond JAN and SPA, to identify a framework that balances the high performance of SPA with the stability of JAN.

The results also demonstrate the importance of the choice of target distribution. In the standard implementation, the GMM target distribution outperforms the Gaussian target distributions across kernelized and adversarial methods, indicating that a Gaussian is not flexible enough to capture the feature distribution. The VAE target distribution is more flexible than the GMM, but more challenging to learn and less stable during training. The numerical results suggest that for a simple dataset like Office31, this trade-off does not favor the VAE distribution, since it fails to outperform the Gaussian. On larger, more complex datasets such as Office-Home, the VAE and the Gaussian are competitive. On the largest dataset, VisDA-2017, the VAE target distribution outperforms the Gaussian when larger amounts of data are present, in the 1% setting, but the Gaussian and GMM perform better on the smallest amount of data in the 0.1% setting. On the other hand, in the SPA framework, the Gaussian distributions outperforms the GMM distribution, perhaps indicating that the training is less sensitive to the choice of target distribution, or less reliant on the Stein discrepancy overall, since it includes several other loss components specific to SPA.

To further explore the affect of the amount of available target data on UDA methods, we evaluate the methods on the Office31 dataset at the following levels of target data: 100%, 75%, 50%, 25%, 10%, 5%, 1%. We include the two highest-performing methods from each implementation: SD-AGMM, SD-KGMM, SPA-SD-KGAU, and SPA-SD-KGMM, as well as benchmark methods. We display the methods on the average across domains in Figure 5; results for each domain individually are included in Figure 9 of Appendix B.

Most methods see a decline in accuracy when the available data is below 10%. The Stein discrepancy-based methods are the most stable with the change of percentages, and have a minimal decline in accuracy as the amount of target data decreases. This suggests that Stein discrepancy-based methods have an advantage when target data is very scarce, which aligns with the results on the VisDA-2017 dataset, which showed little advantage for Stein discrepancy-based methods at the 1% level but significant advantage at the 0.1% level.

5 Conclusion

We have proposed a novel method for UDA based on Stein discrepancy, and derived a theoretical generalization bound that motivates minimizing the Stein discrepancy. The proposed method is adaptable and has both a kernelized form and a non-kernelized, adversarial form, with several possible parametric models for the target distribution: Gaussian, GMM, or VAE. In numerical experiments, our method outperformed baseline methods in the scarce target setting, where only a small amount of target data is available.

Directions for future work include adapting non-parametric KSD from evaluation of implicit generative models to domain adaptation [Xu and Reinert, 2022]. The main advantage is avoiding an explicit score function, eliminating the need to model the target distribution. While the current method benefits from the simplicity of a Gaussian or GMM target distribution, we will assess whether the added flexibility of a non-parametric approach is a worthwhile trade-off. Following Gorham and Mackey [2017], who showed that commonly-used kernels fail to detect non-convergence of distributions in higher dimensions, our future work will investigate the impact of using a kernel such as the inverse multi-quadratic kernel. We will also adapt Stein discrepancy

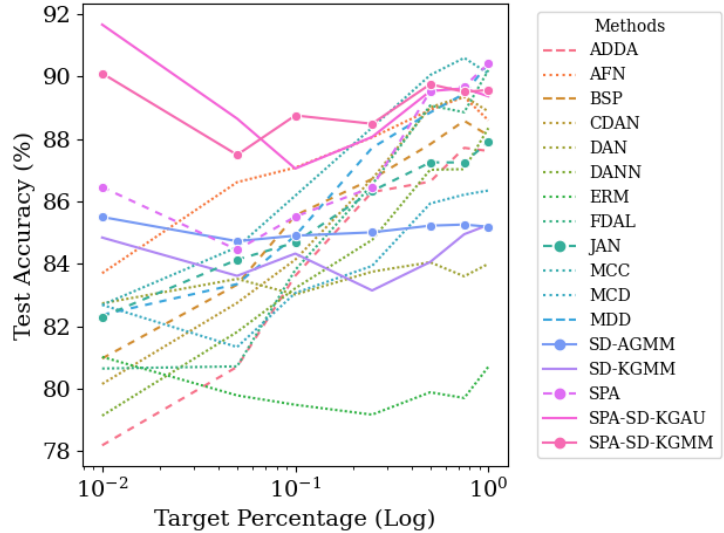


Figure 5: Comparison of methods at different levels of target data on the Office31 dataset, averaged across domains. Stein discrepancy-based methods (solid lines) have a smaller decline in accuracy as the amount of target data is reduced. Methods with circular markers (SD-AGMM, SPA-SD-KGMM, JAN, and SPA) were chosen to help distinguish between Stein discrepancy-based methods that perform similarly, and to highlight the original methods our implementations follow most closely.

to other frameworks, in addition to JAN and SPA. Another avenue for theoretical future work is deriving bounds on the error from replacing the exact Stein discrepancy by an empirical estimate, focusing on the affect of unbalanced sample sizes from the source and target distributions.

Acknowledgements

A.V. and G.L. were partially supported by NSF award DMS 2427955. D.Z. was partially supported by National Natural Science Foundation of China (NSFC) award 12301117.

References

- Kaiming He, Xiangyu Zhang, Shaoqing Ren, and Jian Sun. Delving deep into rectifiers: Surpassing human-level performance on imagenet classification. In *Proceedings of the IEEE international conference on computer vision*, pages 1026–1034, 2015.
- Shai Ben-David, John Blitzer, Koby Crammer, and Fernando Pereira. Analysis of Representations for Domain Adaptation. In B. Schölkopf, J. Platt, and T. Hoffman, editors, *Advances in Neural Information Processing Systems*, volume 19. MIT Press, 2007.
- Shai Ben-David, John Blitzer, Koby Crammer, Alex Kulesza, Fernando Pereira, and Jennifer Wortman Vaughan. A theory of learning from different domains. *Machine Learning*, 79(1-2):151–175, May 2010. ISSN 0885-6125, 1573-0565. doi: 10.1007/s10994-009-5152-4. URL <http://link.springer.com/10.1007/s10994-009-5152-4>.
- Yaroslav Ganin and Victor Lempitsky. Unsupervised Domain Adaptation by Backpropagation. *arXiv:1409.7495 [cs, stat]*, February 2015. URL <http://arxiv.org/abs/1409.7495>. arXiv: 1409.7495.
- Yaroslav Ganin, Evgeniya Ustinova, Hana Ajakan, Pascal Germain, Hugo Larochelle, François Laviolette, Mario Marchand, and Victor Lempitsky. Domain-Adversarial Training of Neural Networks. *arXiv:1505.07818 [cs, stat]*, May 2016. URL <http://arxiv.org/abs/1505.07818>. arXiv: 1505.07818.
- Mingsheng Long, Yue Cao, Jianmin Wang, and Michael I. Jordan. Learning Transferable Features with Deep Adaptation Networks. *arXiv:1502.02791 [cs]*, May 2015. URL <http://arxiv.org/abs/1502.02791>. arXiv: 1502.02791.
- Jian Shen, Yanru Qu, Weinan Zhang, and Yong Yu. Wasserstein Distance Guided Representation Learning for Domain Adaptation. *arXiv:1707.01217 [cs, stat]*, March 2018. URL <http://arxiv.org/abs/1707.01217>. arXiv: 1707.01217.
- Mingsheng Long, Han Zhu, Jianmin Wang, and Michael I. Jordan. Deep Transfer Learning with Joint Adaptation Networks. *arXiv:1605.06636 [cs, stat]*, August 2017. URL <http://arxiv.org/abs/1605.06636>. arXiv: 1605.06636.
- Yufan Shi, Yuhao Wang, and Hua Meng. Single-source unsupervised domain adaptation for cross-subject MI-EEG classification based on discriminative information. *Applied Intelligence*, August 2024. ISSN 1573-7497. doi: 10.1007/s10489-024-05662-0. URL <https://doi.org/10.1007/s10489-024-05662-0>.
- Charles Stein. A bound for the error in the normal approximation to the distribution of a sum of dependent random variables. In *Proceedings of the sixth Berkeley symposium on mathematical statistics and probability, volume 2: Probability theory*, volume 6, pages 583–603. University of California Press, 1972.
- Xiaofeng Liu, Chaehwa Yoo, Fangxu Xing, Hyejin Oh, Georges El Fakhri, Je-Won Kang, Jonghye Woo, et al. Deep unsupervised domain adaptation: A review of recent advances and perspectives. *APSIPA Transactions on Signal and Information Processing*, 11(1), 2022.
- Andreas Anastasiou, Alessandro Barp, François-Xavier Briol, Bruno Ebner, Robert E. Gaunt, Fatemeh Ghaderinezhad, Jackson Gorham, Arthur Gretton, Christophe Ley, Qiang Liu, Lester Mackey, Chris J. Oates, Gesine Reinert, and Yvik Swan. Stein’s Method Meets Computational Statistics: A Review of Some Recent Developments. *Statistical Science*, 38(1):120–139, February 2023. ISSN 0883-4237, 2168-8745. doi: 10.1214/22-STS863. Publisher: Institute of Mathematical Statistics.
- Nicolas Courty, Rémi Flamary, Amaury Habrard, and Alain Rakotomamonjy. Joint Distribution Optimal Transportation for Domain Adaptation. *arXiv:1705.08848 [cs, stat]*, October 2017. URL <http://arxiv.org/abs/1705.08848>. arXiv: 1705.08848.
- Changjian Shui, Qi Chen, Jun Wen, Fan Zhou, Christian Gagné, and Boyu Wang. A novel domain adaptation theory with Jensen–Shannon divergence. *Knowledge-Based Systems*, 257:109808, December 2022. ISSN 0950-7051. doi: 10.1016/j.knosys.2022.109808. URL <https://www.sciencedirect.com/science/article/pii/S0950705122009200>.

- Yishay Mansour, Mehryar Mohri, and Afshin Rostamizadeh. Multiple source adaptation and the rényi divergence. In *Proceedings of the Twenty-Fifth Conference on Uncertainty in Artificial Intelligence*, pages 367–374, 2009.
- A Tuan Nguyen, Toan Tran, Yarin Gal, Philip Torr, and Atilim Gunes Baydin. Kl guided domain adaptation. In *International Conference on Learning Representations*, 2022.
- Artem Rozantsev, Mathieu Salzmann, and Pascal Fua. Beyond sharing weights for deep domain adaptation. *IEEE transactions on pattern analysis and machine intelligence*, 41(4):801–814, 2018.
- Ming-Yu Liu and Onel Tuzel. Coupled Generative Adversarial Networks. In D. Lee, M. Sugiyama, U. Luxburg, I. Guyon, and R. Garnett, editors, *Advances in Neural Information Processing Systems*, volume 29. Curran Associates, Inc., 2016.
- Yuchen Zhang, Tianle Liu, Mingsheng Long, and Michael Jordan. Bridging Theory and Algorithm for Domain Adaptation. In *Proceedings of the 36th International Conference on Machine Learning*, pages 7404–7413. PMLR, May 2019. URL <https://proceedings.mlr.press/v97/zhang19i.html>. ISSN: 2640-3498.
- Mingsheng Long, Zhangjie Cao, Jianmin Wang, and Michael I Jordan. Conditional Adversarial Domain Adaptation. In S. Bengio, H. Wallach, H. Larochelle, K. Grauman, N. Cesa-Bianchi, and R. Garnett, editors, *Advances in Neural Information Processing Systems*, volume 31. Curran Associates, Inc., 2018.
- David Acuna, Guojun Zhang, Marc T Law, and Sanja Fidler. f-domain adversarial learning: Theory and algorithms. In *International Conference on Machine Learning*, pages 66–75. PMLR, 2021.
- Boqing Gong, Kristen Grauman, and Fei Sha. Connecting the dots with landmarks: Discriminatively learning domain-invariant features for unsupervised domain adaptation. In Sanjoy Dasgupta and David McAllester, editors, *Proceedings of the 30th International Conference on Machine Learning*, volume 28 of *Proceedings of Machine Learning Research*, pages 222–230, Atlanta, Georgia, USA, 17–19 Jun 2013. PMLR. URL <https://proceedings.mlr.press/v28/gong13.html>.
- Mingsheng Long, Jianmin Wang, Guiguang Ding, Jianguang Sun, and Philip S. Yu. Transfer joint matching for unsupervised domain adaptation. In *Proceedings of the IEEE Conference on Computer Vision and Pattern Recognition (CVPR)*, June 2014.
- Kihyuk Sohn, David Berthelot, Nicholas Carlini, Zizhao Zhang, Han Zhang, Colin A Raffel, Ekin Dogus Cubuk, Alexey Kurakin, and Chun-Liang Li. Fixmatch: Simplifying semi-supervised learning with consistency and confidence. *Advances in neural information processing systems*, 33:596–608, 2020.
- Fuxiang Huang, Suqi Song, and Lei Zhang. Gradient Harmonization in Unsupervised Domain Adaptation. *IEEE Transactions on Pattern Analysis and Machine Intelligence*, pages 1–17, 2024. ISSN 1939-3539. doi: 10.1109/TPAMI.2024.3438154. URL <https://ieeexplore.ieee.org/abstract/document/10623315>. Conference Name: IEEE Transactions on Pattern Analysis and Machine Intelligence.
- Zhiqing Xiao, Haobo Wang, Ying Jin, Lei Feng, Gang Chen, Fei Huang, and Junbo Zhao. Spa: a graph spectral alignment perspective for domain adaptation. *Advances in Neural Information Processing Systems*, 36, 2024.
- Sicheng Zhao, Bo Li, Colorado Reed, Pengfei Xu, and Kurt Keutzer. Multi-source domain adaptation in the deep learning era: A systematic survey, 2020. URL <https://arxiv.org/abs/2002.12169>.
- Pau Panareda Busto and Juergen Gall. Open Set Domain Adaptation. pages 754–763, 2017. URL https://openaccess.thecvf.com/content_iccv_2017/html/Busto_Open_Set_Domain_ICCV_2017_paper.html.
- Jindong Wang, Cuiling Lan, Chang Liu, Yidong Ouyang, Tao Qin, Wang Lu, Yiqiang Chen, Wenjun Zeng, and Philip Yu. Generalizing to Unseen Domains: A Survey on Domain Generalization. *IEEE Transactions on Knowledge and Data Engineering*, pages 1–1, 2022. ISSN 1041-4347, 1558-2191, 2326-3865. doi: 10.1109/TKDE.2022.3178128. URL <https://ieeexplore.ieee.org/document/9782500/>.
- Archit Parnami and Minwoo Lee. Learning from few examples: A summary of approaches to few-shot learning. *arXiv preprint arXiv:2203.04291*, 2022.
- Jackson Gorham and Lester Mackey. Measuring Sample Quality with Stein’s Method. In *Advances in Neural Information Processing Systems*, volume 28. Curran Associates, Inc., 2015.
- Jackson Gorham and Lester Mackey. Measuring sample quality with kernels. In *International Conference on Machine Learning*, pages 1292–1301. PMLR, 2017.
- Qiang Liu, Jason D. Lee, and Michael I. Jordan. A Kernelized Stein Discrepancy for Goodness-of-fit Tests and Model Evaluation. *arXiv:1602.03253 [stat]*, July 2016. URL <http://arxiv.org/abs/1602.03253>. arXiv: 1602.03253.
- Kacper Chwialkowski, Heiko Strathmann, and Arthur Gretton. A Kernel Test of Goodness of Fit. In *Proceedings of The 33rd International Conference on Machine Learning*, pages 2606–2615. PMLR, June 2016. URL <https://proceedings.mlr.press/v48/chwialkowski16.html>. ISSN: 1938-7228.

- Qiang Liu and Dilin Wang. Stein Variational Gradient Descent: A General Purpose Bayesian Inference Algorithm, September 2019. URL <http://arxiv.org/abs/1608.04471>. arXiv:1608.04471 [cs, stat].
- Wilson Ye Chen, Lester Mackey, Jackson Gorham, François-Xavier Briol, and Chris Oates. Stein points. In *International Conference on Machine Learning*, pages 844–853. PMLR, 2018.
- Marina Riabiz, Wilson Ye Chen, Jon Cockayne, Pawel Swietach, Steven A Niederer, Lester Mackey, and Chris J Oates. Optimal thinning of mcmc output. *Journal of the Royal Statistical Society Series B: Statistical Methodology*, 84(4): 1059–1081, 2022.
- Wenkai Xu and Gesine D. Reinert. A Kernelised Stein Statistic for Assessing Implicit Generative Models. *Advances in Neural Information Processing Systems*, 35:7277–7289, December 2022.
- Calvin Luo. Understanding Diffusion Models: A Unified Perspective, August 2022. URL <http://arxiv.org/abs/2208.11970>. arXiv:2208.11970 [cs].
- Kate Saenko, Brian Kulis, Mario Fritz, and Trevor Darrell. Adapting visual category models to new domains. In *Computer Vision—ECCV 2010: 11th European Conference on Computer Vision, Heraklion, Crete, Greece, September 5–11, 2010, Proceedings, Part IV 11*, pages 213–226. Springer, 2010.
- Hemanth Venkateswara, Jose Eusebio, Shayok Chakraborty, and Sethuraman Panchanathan. Deep hashing network for unsupervised domain adaptation. In *Proceedings of the IEEE conference on computer vision and pattern recognition*, pages 5018–5027, 2017.
- Xingchao Peng, Ben Usman, Neela Kaushik, Judy Hoffman, Dequan Wang, and Kate Saenko. Visda: The visual domain adaptation challenge. *arXiv preprint arXiv:1710.06924*, 2017.
- Eric Tzeng, Judy Hoffman, Kate Saenko, and Trevor Darrell. Adversarial discriminative domain adaptation. In *Proceedings of the IEEE Conference on Computer Vision and Pattern Recognition (CVPR)*, July 2017.
- Xinyang Chen, Sinan Wang, Mingsheng Long, and Jianmin Wang. Transferability vs. discriminability: Batch spectral penalization for adversarial domain adaptation. In *ICML*, 2019.
- Ruijia Xu, Guanbin Li, Jihan Yang, and Liang Lin. Larger norm more transferable: An adaptive feature norm approach for unsupervised domain adaptation. In *ICCV*, 2019.
- Kuniaki Saito, Kohei Watanabe, Yoshitaka Ushiku, and Tatsuya Harada. Maximum classifier discrepancy for unsupervised domain adaptation. In *CVPR*, 2018.
- Ying Jin, Ximei Wang, Mingsheng Long, and Jianmin Wang. Less confusion more transferable: Minimum class confusion for versatile domain adaptation. In *ECCV*, 2020.
- Junguang Jiang, Baixu Chen, Bo Fu, and Mingsheng Long. Transfer-learning-library. <https://github.com/thuml/Transfer-Learning-Library>, 2020.
- Junguang Jiang, Yang Shu, Jianmin Wang, and Mingsheng Long. Transferability in deep learning: A survey, 2022.
- Kaiming He, Xiangyu Zhang, Shaoqing Ren, and Jian Sun. Deep residual learning for image recognition. In *Proceedings of the IEEE conference on computer vision and pattern recognition*, pages 770–778, 2016.
- Anna Korba, Pierre-Cyril Aubin-Frankowski, Szymon Majewski, and Pierre Ablin. Kernel Stein Discrepancy Descent, May 2021. URL <http://arxiv.org/abs/2105.09994>. arXiv:2105.09994 [cs, stat].
- James Bergstra, Daniel Yamins, and David Cox. Making a science of model search: Hyperparameter optimization in hundreds of dimensions for vision architectures. In *International conference on machine learning*, pages 115–123. PMLR, 2013.
- Richard Liaw, Eric Liang, Robert Nishihara, Philipp Moritz, Joseph E Gonzalez, and Ion Stoica. Tune: A research platform for distributed model selection and training. *arXiv preprint arXiv:1807.05118*, 2018.
- Arthur Gretton, Karsten M. Borgwardt, Malte J. Rasch, Bernhard Schölkopf, and Alexander Smola. A Kernel Two-Sample Test. *Journal of Machine Learning Research*, 13(25):723–773, 2012. ISSN 1533-7928. URL <http://jmlr.org/papers/v13/gretton12a.html>.

A Proof of Theorem 3.2

Proof. We first show that KSD can be viewed as a special case of squared MMD. Since KSD provides the exact Stein discrepancy when maximizing over a RKHS, showing the relationship between KSD and MMD establishes the bound for the general Stein discrepancy.

Since \mathcal{F} is the unit ball of an RKHS, the MMD between \mathcal{D}_S and \mathcal{D}_T can be written as

$$d_{\text{MMD}}(\mathcal{D}_S, \mathcal{D}_T) = \sup_{f \in \mathcal{F}} |\mathbb{E}_{x \sim \mathcal{D}_S}[f(x)] - \mathbb{E}_{x \sim \mathcal{D}_T}[f(x)]|.$$

Moreover, Gretton et al. [2012] showed that the squared MMD can be written in a kernelized form

$$d_{\text{MMD}}^2(\mathcal{D}_S, \mathcal{D}_T) = \mathbb{E}_{x, x' \sim \mathcal{D}_S}[k(x, x')] - 2\mathbb{E}_{x \sim \mathcal{D}_S, y \sim \mathcal{D}_T}[k(x, y)] + \mathbb{E}_{y, y' \sim \mathcal{D}_T}[k(y, y')].$$

Liu et al. [2016] verified that $\mathcal{A}_{\mathcal{D}_T} \mathcal{A}_{\mathcal{D}_T} k(x, x')$ is a valid positive definite kernel and is contained in the Stein class of \mathcal{D}_S , as long as the same is true for $k(x, x')$. Using Stein’s identity, which states that $\mathbb{E}_q[\mathcal{A}_q f(x)] = 0$, it follows that the squared MMD and Stein discrepancy are equivalent:

$$\begin{aligned} d_{\text{MMD}}^2(\mathcal{D}_S, \mathcal{D}_T) &= \mathbb{E}_{x, x' \sim \mathcal{D}_S}[\mathcal{A}_{\mathcal{D}_T} \mathcal{A}_{\mathcal{D}_T} k(x, x')] \\ &\quad - 2\mathbb{E}_{x \sim \mathcal{D}_S} \mathbb{E}_{y \sim \mathcal{D}_T}[\mathcal{A}_{\mathcal{D}_T} \mathcal{A}_{\mathcal{D}_T} k(x, y)] \\ &\quad + \mathbb{E}_{y \sim \mathcal{D}_T} \mathbb{E}_{y' \sim \mathcal{D}_T}[\mathcal{A}_{\mathcal{D}_T} \mathcal{A}_{\mathcal{D}_T} k(y, y')] \\ &= \mathbb{E}_{x, x' \sim \mathcal{D}_S}[\mathcal{A}_{\mathcal{D}_T} \mathcal{A}_{\mathcal{D}_T} k(x, x')] \\ &\quad - 2\mathbb{E}_{x \sim \mathcal{D}_S}[0] + \mathbb{E}_{y \sim \mathcal{D}_T}[0] \\ &= \mathbb{E}_{x, x' \sim \mathcal{D}_S}[\mathcal{A}_{\mathcal{D}_T} \mathcal{A}_{\mathcal{D}_T} k(x, x')] \\ &= S(\mathcal{D}_S, \mathcal{D}_T). \end{aligned}$$

The proof follows from combining the above equation and the result of Long et al. [2015], which states that

$$\epsilon_T(f) \leq \epsilon_S(f) + 2d_{\text{MMD}}(\mathcal{D}_S, \mathcal{D}_T) + C,$$

where C depends on the VC dimension of \mathcal{F} , the sample size from each distribution, and the smallest possible test errors in both domains. \square

B Additional Experimental Results

More detailed experimental results are provided here. We provide figures illustrating results of the full target setting, where we use all the available target data in each dataset, to complement the figures of the scarce target setting provided in the main text. Figures 6, 7, and 8 show the accuracy in the full target setting for the Office31, Office-Home, and VisDA-2017 datasets respectively. Together, these figures provide a summary of the results across all possible domain pairs in each dataset (6 pairs in Office31, 12 pairs in Office-Home, 1 pair in VisDA2017).

In addition, we also provide tables that show the accuracy and standard deviation on each domain pair. On individual domains, the accuracy reported is the highest accuracy achieved by each method, and the standard deviation is taken across the three highest performing model runs. The accuracy reported averaged across domain is an average of the three top model runs on each domain, and the pooled standard deviation across domains is reported. The results for Office31 are given in Tables 1-3, for Office-Home in Tables 4-6, and for VisDA-2017 in Table 7. The highest accuracy for each domain is bolded and the second-highest is underlined. The “Full” column refers to training on all of the available target data, the “Scarce” column refers to the scarce target setting, in which the model was trained on 1% of the available target data, with a minimum of 32 samples of target data. VisDA-2017 contains the most samples per domain in the target domain (approximately 55,000), so we report accuracy on 100%, 1% and 0.1% of target data to ensure that the scarce target setting is represented.

Finally, since Figure 5 in the main text only includes the average performance across all domains in the Office31 dataset, we provide a more detailed breakdown in Figure 9, which displays the performance on each domain individually. We report the highest performing model run on each target percentage for each method.

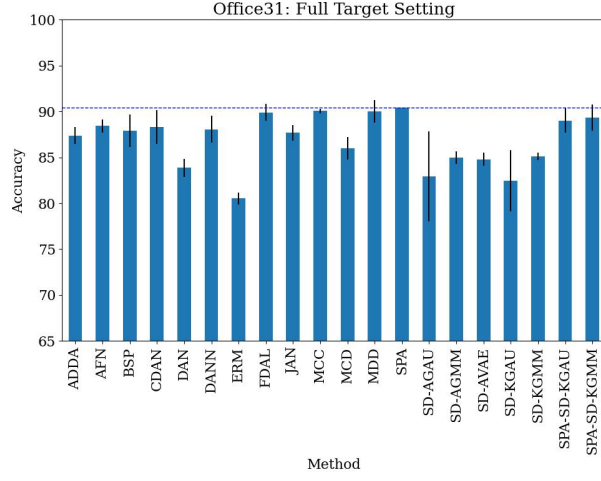


Figure 6: Average accuracy across domains and pooled standard deviation on Office31 dataset in full target setting (trained on 100% of available target data). Horizontal line denotes the highest accuracy.

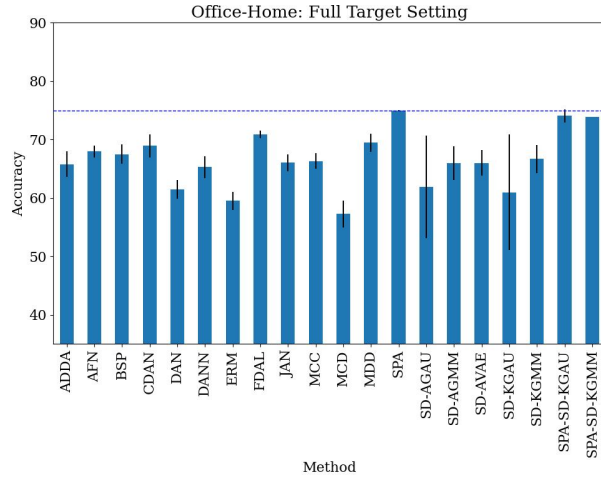


Figure 7: Average accuracy across domains and pooled standard deviation on Office-Home dataset in full target setting (trained on 100% of available target data). Horizontal line denotes the highest accuracy.

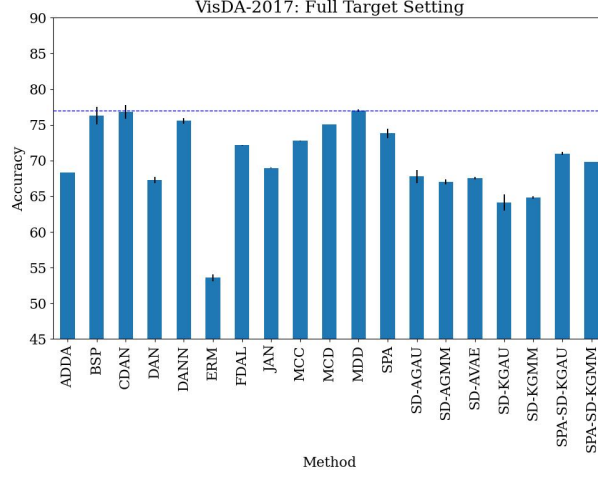


Figure 8: Average accuracy across domains and pooled standard deviation on VisDA-2017 dataset in full target setting (trained on 100% of available target data). Horizontal line denotes the highest accuracy.

Table 1: Accuracy on Office31 dataset, averaged across six domain pairs. Full refers to accuracy trained on full target dataset; scarce refers to accuracy trained in scarce target setting (32 target samples).

Method	Full	Scarce
ADDA	87.62 (0.93)	78.18 (3.37)
AFN	88.60 (0.73)	83.70 (2.11)
BSP	88.12 (1.77)	80.97 (1.77)
CDAN	88.88 (1.86)	80.15 (1.35)
DAN	84.00 (0.99)	82.73 (1.33)
DANN	88.35 (1.44)	79.13 (3.08)
ERM	80.70 (0.63)	81.02 (0.86)
FDAL	90.21 (0.90)	80.65 (4.65)
JAN	87.90 (0.87)	82.30 (1.32)
MCC	90.10 (0.24)	82.68 (1.71)
MCD	86.35 (1.23)	82.68 (2.49)
MDD	90.42 (1.21)	82.37 (2.30)
SPA	90.42 (0.00)	86.46 (7.87)
SD-AGAU	84.39 (4.87)	81.98 (1.31)
SD-AGMM	85.19 (0.67)	85.50 (1.13)
SD-AVAE	85.00 (0.69)	81.83 (2.38)
SD-KGAU	83.56 (3.33)	81.42 (2.10)
SD-KGMM	85.25 (0.42)	84.84 (2.40)
SPA-SD-KGAU	89.37 (1.33)	91.67 (3.61)
SPA-SD-KGMM	89.57 (1.43)	<u>90.11 (5.99)</u>

Table 2: Accuracy and standard deviation on Office31 in the full target setting (100% of target data available). The best accuracy is bolded and the second best is underlined.

Method	A2D	A2W	D2A	D2W	W2A	W2D	mean
ADDA	92.2 (0.83)	92.7 (0.21)	70.0 (0.23)	97.7 (0.06)	73.1 (0.23)	100.0 (0.12)	87.62
AFN	95.2 (0.23)	92.8 (0.38)	73.5 (0.57)	99.0 (0.06)	71.1 (0.06)	100.0 (0.00)	88.60
BSP	89.0 (1.77)	92.7 (0.00)	73.9 (0.00)	98.2 (0.00)	74.9 (0.00)	100.0 (0.00)	88.12
CDAN	92.2 (1.30)	95.1 (0.61)	74.5 (0.45)	99.0 (0.21)	72.5 (1.08)	100.0 (0.00)	88.88
DAN	88.6 (0.98)	85.5 (0.06)	66.6 (0.12)	98.7 (0.06)	64.6 (0.06)	100.0 (0.00)	84.00
DANN	86.9 (0.81)	94.0 (0.75)	75.2 (0.46)	98.2 (0.06)	<u>76.0 (0.81)</u>	99.8 (0.00)	88.35
ERM	82.1 (0.31)	77.7 (0.51)	64.1 (0.06)	96.7 (0.10)	64.4 (0.15)	99.2 (0.00)	80.70
FDAL	<u>95.6 (0.31)</u>	95.0 (0.44)	76.1 (0.43)	99.0 (0.13)	75.6 (0.56)	100.0 (0.00)	90.21
JAN	90.8 (0.42)	95.0 (0.45)	71.1 (0.06)	98.2 (0.06)	72.3 (0.61)	100.0 (0.00)	87.90
MCC	97.4 (0.00)	94.2 (0.23)	75.6 (0.00)	98.5 (0.06)	75.1 (0.00)	<u>99.8 (0.00)</u>	90.10
MCD	90.2 (0.53)	91.3 (0.75)	70.1 (0.70)	98.6 (0.12)	67.9 (0.40)	<u>100.0 (0.00)</u>	86.35
MDD	95.4 (0.58)	96.5 (0.51)	77.3 (0.82)	99.1 (0.06)	74.2 (0.44)	100.0 (0.00)	90.42
SPA	94.0 (0.00)	94.7 (0.00)	77.5 (0.00)	98.9 (0.00)	77.9 (0.00)	99.6 (0.00)	<u>90.42</u>
SD-AGAU	87.8 (1.34)	83.3 (3.92)	68.4 (0.39)	98.1 (0.26)	68.8 (2.52)	100.0 (0.00)	84.39
SD-AGMM	88.6 (0.53)	84.5 (0.13)	68.8 (0.16)	99.0 (0.13)	70.3 (0.34)	100.0 (0.00)	85.19
SD-AVAE	88.0 (0.12)	85.3 (0.29)	68.9 (0.58)	99.2 (0.15)	68.7 (0.16)	100.0 (0.00)	85.00
SD-KGAU	88.2 (2.63)	80.0 (1.69)	68.5 (0.57)	98.5 (0.15)	66.2 (0.96)	100.0 (0.00)	83.56
SD-KGMM	89.0 (0.31)	84.3 (0.07)	69.2 (0.04)	99.0 (0.22)	70.1 (0.16)	100.0 (0.00)	85.25
SPA-SD-KGAU	95.4 (0.46)	94.0 (1.16)	75.3 (0.39)	99.0 (0.00)	73.2 (0.18)	99.4 (0.12)	89.37
SPA-SD-KGMM	94.0 (0.12)	94.1 (1.38)	75.3 (0.15)	99.0 (0.07)	75.4 (0.30)	99.6 (0.12)	89.57

Table 3: Accuracy and standard deviation on Office31 in the scarce target setting (32 training samples available; all domains are small enough that 1% of target data would be less than 32 samples). The best accuracy is bolded and the second best is underlined.

Method	A2D	A2W	D2A	D2W	W2A	W2D	mean
ADDA	78.7 (1.63)	78.1 (1.15)	60.2 (0.85)	95.0 (2.36)	59.9 (0.51)	97.2 (0.87)	78.18
AFN	86.3 (0.70)	84.4 (0.71)	67.8 (1.64)	98.1 (0.31)	65.6 (0.06)	100.0 (0.81)	83.70
BSP	83.1 (1.33)	78.5 (0.40)	64.3 (0.70)	97.7 (0.53)	62.4 (0.66)	99.8 (0.00)	80.97
CDAN	80.9 (0.64)	79.5 (0.78)	63.6 (0.23)	97.6 (0.13)	59.5 (0.82)	<u>99.8 (0.23)</u>	80.15
DAN	86.1 (0.90)	81.3 (0.47)	66.3 (0.61)	98.5 (0.46)	64.2 (0.38)	<u>100.0 (0.00)</u>	82.73
DANN	79.3 (0.64)	79.2 (2.70)	61.2 (0.90)	97.1 (0.50)	58.2 (0.75)	99.8 (0.42)	79.13
ERM	82.3 (0.31)	77.7 (0.64)	64.6 (0.38)	96.9 (0.17)	65.0 (0.10)	99.6 (0.23)	81.02
FDAL	83.7 (2.81)	78.4 (3.21)	64.1 (0.81)	94.5 (0.80)	66.8 (1.36)	96.4 (0.46)	80.65
JAN	84.7 (0.50)	81.9 (0.99)	64.9 (0.25)	97.7 (0.06)	64.6 (0.57)	100.0 (0.35)	82.30
MCC	85.5 (1.10)	82.1 (0.44)	65.5 (0.91)	98.6 (0.55)	64.4 (0.55)	100.0 (0.31)	82.68
MCD	84.3 (0.50)	85.9 (2.34)	64.3 (0.32)	98.0 (0.06)	63.8 (0.60)	99.8 (0.12)	82.68
MDD	88.0 (2.08)	81.3 (0.80)	64.6 (0.18)	98.5 (0.23)	61.8 (0.44)	100.0 (0.12)	82.37
SPA	90.6 (3.12)	84.4 (1.81)	71.9 (3.13)	100.0 (0.00)	71.9 (6.25)	100.0 (0.00)	86.46
SD-AGAU	83.9 (0.64)	82.6 (1.07)	64.1 (0.06)	97.9 (0.35)	63.4 (0.10)	100.0 (0.12)	81.98
SD-AGMM	88.6 (0.72)	85.2 (0.44)	70.3 (0.55)	<u>98.6 (0.07)</u>	70.4 (0.50)	100.0 (0.00)	85.50
SD-AVAE	85.9 (1.93)	77.7 (0.59)	66.1 (1.07)	<u>98.6 (0.32)</u>	62.5 (0.58)	100.0 (0.00)	81.83
SD-KGAU	82.3 (1.34)	80.0 (1.40)	68.5 (0.57)	98.2 (0.07)	59.4 (0.58)	100.0 (0.00)	81.42
SD-KGMM	87.8 (2.35)	84.3 (0.29)	68.7 (0.37)	98.6 (0.07)	69.7 (0.07)	100.0 (0.00)	84.84
SPA-SD-KGAU	93.8 (1.81)	90.6 (1.80)	84.4 (1.81)	100.0 (0.00)	81.2 (1.81)	100.0 (0.00)	91.67
SPA-SD-KGMM	<u>93.8 (1.81)</u>	<u>90.6 (3.12)</u>	71.9 (3.13)	100.0 (0.00)	84.4 (3.61)	100.0 (0.00)	<u>90.11</u>

Table 4: Accuracy on Office-Home, averaged across 12 domain pairs. Full refers to accuracy trained on full target dataset (100% of available data); scarce refers to accuracy trained in scarce target setting (minimum of 1% of target data or 32 samples).

Method	Full	Scarce
ADDA	66.29 (2.20)	54.65 (12.33)
AFN	68.23 (0.99)	65.28 (2.14)
BSP	67.81 (1.67)	59.48 (3.12)
CDAN	69.33 (1.97)	57.52 (1.85)
DAN	61.79 (1.57)	61.22 (2.76)
DANN	65.67 (1.87)	56.76 (4.08)
ERM	59.81 (1.57)	59.68 (1.16)
FDAL	71.01 (0.62)	61.73 (2.15)
JAN	66.33 (1.46)	61.27 (2.85)
MCC	66.58 (1.33)	57.67 (1.62)
MCD	57.69 (2.28)	59.37 (2.45)
MDD	69.79 (1.54)	59.05 (3.95)
SPA	74.93 (0.11)	70.89 (11.09)
SD-AGAU	63.68 (8.74)	65.67 (3.54)
SD-AGMM	66.48 (2.87)	65.47 (2.15)
SD-AVAE	66.50 (2.22)	65.79 (6.16)
SD-KGAU	63.37 (9.87)	63.10 (4.04)
SD-KGMM	67.12 (2.43)	65.11 (1.42)
SPA-SD-KGAU	74.27 (1.13)	72.99 (11.90)
SPA-SD-KGMM	73.93 (0.00)	<u>72.35 (14.80)</u>

Table 5: Results on OfficeHome dataset in full target setting (trained on 100% of target data). The first six domain pairs are shown in the top half of the table; the remaining six appear in the bottom half.

Method	Ar2Cl	Cl2Ar	Ar2Rw	Ar2Pr	Cl2Rw	Cl2Pr
ADDA	52.9 (0.53)	59.8 (0.57)	75.1 (0.36)	68.0 (1.32)	69.1 (0.23)	68.6 (0.87)
AFN	53.4 (0.25)	65.2 (0.21)	77.4 (0.29)	72.9 (0.40)	72.3 (0.00)	71.3 (0.10)
BSP	54.0 (0.00)	60.2 (0.40)	76.8 (0.07)	68.3 (0.70)	70.7 (0.15)	70.8 (0.64)
CDAN	54.8 (31.55)	62.1 (0.44)	78.6 (0.21)	72.0 (0.10)	71.7 (0.74)	71.6 (0.07)
DAN	46.0 (0.64)	56.9 (0.65)	74.4 (0.35)	68.3 (0.21)	66.9 (0.25)	64.3 (0.42)
DANN	53.3 (0.49)	56.4 (0.23)	74.0 (0.14)	63.1 (0.15)	69.1 (0.49)	66.6 (0.57)
ERM	44.4 (0.07)	53.2 (0.17)	74.4 (0.28)	68.2 (0.70)	64.1 (0.32)	62.2 (0.14)
FDAL	56.1 (0.13)	64.7 (0.31)	81.5 (0.12)	75.5 (0.31)	75.0 (0.09)	74.7 (0.06)
JAN	50.8 (0.35)	60.1 (0.15)	77.1 (0.07)	71.7 (0.30)	69.9 (0.46)	68.1 (0.21)
MCC	50.2 (0.57)	50.1 (0.64)	80.8 (0.21)	78.7 (0.14)	68.9 (0.44)	68.6 (0.14)
MCD	41.9 (0.99)	50.4 (1.10)	73.1 (0.28)	63.5 (0.72)	61.6 (0.50)	58.1 (0.99)
MDD	56.0 (0.21)	63.0 (0.38)	79.6 (0.64)	75.2 (0.36)	73.8 (0.31)	73.1 (0.49)
SPA	59.8 (0.00)	72.1 (0.00)	84.8 (0.00)	80.4 (0.00)	81.6 (0.11)	80.2 (0.00)
SD-AGAU	51.5 (0.30)	63.8 (0.90)	64.6 (1.70)	71.2 (1.16)	64.9 (7.30)	60.5 (2.13)
SD-AGMM	50.7 (0.19)	64.5 (0.52)	76.2 (0.79)	71.7 (2.14)	69.5 (0.26)	65.6 (1.51)
SD-AVAE	49.3 (1.72)	63.2 (0.32)	78.1 (0.21)	72.0 (0.44)	69.8 (0.40)	66.5 (0.87)
SD-KGAU	49.8 (2.66)	55.8 (3.78)	75.3 (3.53)	70.8 (6.83)	71.4 (0.96)	56.0 (0.19)
SD-KGMM	51.1 (0.23)	64.8 (0.70)	78.6 (0.15)	71.8 (0.31)	72.9 (0.78)	69.4 (0.78)
SPA-SD-KGAU	59.0 (0.07)	71.9 (0.40)	84.6 (0.06)	80.6 (0.09)	81.5 (0.41)	79.4 (0.00)
SPA-SD-KGMM	<u>58.1 (0.00)</u>	<u>71.4 (0.00)</u>	<u>84.6 (0.00)</u>	81.2 (0.00)	<u>80.9 (0.00)</u>	<u>79.3 (0.00)</u>

Method	Pr2Cl	Pr2Ar	Pr2Rw	Rw2Ar	Rw2Cl	Rw2Pr
ADDA	54.7 (0.81)	61.3 (0.50)	77.5 (0.29)	70.6 (0.31)	58.1 (0.66)	79.8 (0.10)
AFN	52.0 (0.50)	64.5 (0.42)	77.9 (0.21)	72.5 (0.23)	57.6 (0.25)	81.8 (0.21)
BSP	55.7 (0.62)	62.6 (0.14)	79.8 (0.49)	73.0 (0.52)	60.3 (0.07)	81.5 (0.88)
CDAN	55.8 (0.65)	63.9 (0.95)	80.8 (0.28)	74.6 (0.40)	61.6 (1.13)	84.5 (0.45)
DAN	40.4 (0.38)	55.2 (0.71)	74.5 (0.49)	67.1 (0.35)	49.0 (0.42)	78.5 (0.15)
DANN	55.2 (1.27)	57.6 (0.57)	78.9 (0.57)	71.4 (0.45)	61.1 (0.07)	81.4 (0.35)
ERM	39.6 (0.44)	53.2 (1.15)	72.9 (0.07)	64.8 (0.25)	44.4 (0.21)	76.3 (0.30)
FDAL	54.7 (0.15)	66.4 (0.13)	82.4 (0.01)	75.2 (0.07)	60.2 (0.31)	85.8 (0.01)
JAN	50.5 (0.81)	61.6 (0.42)	77.5 (0.14)	71.6 (0.15)	55.9 (0.78)	81.1 (0.38)
MCC	42.8 (0.75)	62.1 (0.21)	81.0 (0.07)	74.4 (0.21)	56.4 (0.21)	84.9 (0.25)
MCD	36.4 (0.83)	50.6 (0.07)	72.3 (0.14)	64.7 (0.26)	44.0 (0.07)	75.7 (0.60)
MDD	54.7 (0.32)	63.8 (0.99)	79.8 (0.14)	73.8 (0.21)	60.3 (0.21)	84.4 (0.35)
SPA	58.2 (0.00)	<u>71.2 (0.00)</u>	85.0 (0.00)	77.4 (0.00)	60.5 (0.00)	<u>88.0 (0.00)</u>
SD-AGAU	47.0 (0.89)	65.3 (1.08)	69.5 (3.29)	73.1 (0.60)	52.0 (0.32)	80.8 (0.32)
SD-AGMM	47.5 (0.13)	65.5 (0.26)	78.7 (0.12)	73.6 (0.28)	53.4 (0.34)	80.7 (0.26)
SD-AVAE	47.0 (0.29)	65.9 (0.11)	79.2 (0.59)	73.4 (0.27)	52.5 (0.33)	81.0 (0.27)
SD-KGAU	42.9 (0.88)	62.9 (1.83)	78.8 (1.27)	66.8 (0.73)	51.0 (1.73)	78.9 (2.61)
SD-KGMM	47.3 (0.66)	65.1 (1.83)	78.4 (0.14)	73.1 (0.42)	51.9 (0.19)	81.1 (0.09)
SPA-SD-KGAU	54.5 (0.00)	72.2 (0.93)	84.7 (0.00)	75.8 (0.00)	59.0 (0.00)	88.1 (0.25)
SPA-SD-KGMM	54.6 (0.00)	70.5 (0.00)	84.1 (0.00)	75.6 (0.00)	59.4 (0.00)	87.3 (0.00)

Table 6: Results on OfficeHome dataset in scarce target setting (trained on minimum of 1% of target data or 32 samples). The first six domain pairs are shown in the top half of the table; the remaining six appear in the bottom half.

Method	Ar2Cl	Cl2Ar	Ar2Rw	Ar2Pr	Cl2Rw	Cl2Pr
ADDA	40.4 (2.64)	52.6 (3.25)	68.0 (7.38)	57.1 (3.15)	58.8 (7.39)	57.4 (2.35)
AFN	50.7 (0.47)	60.5 (0.98)	76.6 (0.21)	70.3 (0.75)	70.8 (0.49)	68.8 (0.90)
BSP	44.4 (0.50)	52.9 (0.92)	73.2 (1.35)	63.8 (0.64)	63.8 (0.35)	60.7 (0.92)
CDAN	41.6 (0.21)	48.2 (0.26)	71.8 (0.67)	63.6 (0.92)	60.9 (0.35)	57.8 (0.21)
DAN	45.8 (0.70)	56.7 (1.00)	74.2 (0.25)	67.4 (0.85)	67.1 (1.13)	63.2 (0.12)
DANN	41.6 (0.32)	48.5 (0.71)	70.9 (1.10)	63.0 (1.56)	59.7 (0.57)	57.5 (1.25)
ERM	44.6 (0.49)	52.6 (0.46)	75.1 (0.55)	67.4 (0.28)	64.0 (0.28)	62.4 (0.15)
FDAL	44.7 (0.92)	55.4 (0.17)	77.4 (0.41)	67.8 (0.41)	66.2 (0.52)	63.7 (0.20)
JAN	45.5 (0.68)	55.0 (1.27)	75.3 (0.56)	67.5 (0.99)	65.6 (0.99)	62.1 (0.30)
MCC	41.8 (0.32)	48.9 (0.57)	73.0 (0.21)	63.7 (0.42)	58.9 (0.24)	59.3 (0.62)
MCD	43.1 (0.64)	54.3 (2.26)	73.5 (0.06)	64.1 (0.21)	64.9 (0.00)	60.0 (0.21)
MDD	43.3 (1.21)	53.4 (0.71)	72.9 (0.46)	65.2 (0.85)	64.6 (3.24)	61.5 (0.67)
SPA	62.8 (3.55)	<u>71.9 (3.13)</u>	86.0 (2.68)	81.8 (4.73)	<u>72.1 (4.65)</u>	59.1 (1.31)
SD-AGAU	49.1 (0.23)	63.2 (1.17)	77.5 (0.97)	71.6 (2.23)	68.9 (2.11)	64.7 (0.51)
SD-AGMM	50.4 (0.21)	63.1 (0.55)	76.8 (0.19)	68.6 (0.24)	66.4 (0.71)	65.3 (0.96)
SD-AVAE	49.8 (4.91)	61.3 (0.31)	77.0 (0.21)	71.4 (2.78)	70.4 (0.56)	65.9 (0.28)
SD-KGAU	48.3 (2.19)	64.7 (1.03)	74.1 (2.26)	66.7 (0.53)	64.8 (1.07)	60.6 (1.71)
SD-KGMM	48.5 (0.79)	63.2 (0.27)	78.1 (0.58)	72.0 (0.14)	68.1 (0.49)	65.9 (0.25)
SPA-SD-KGAU	60.5 (4.03)	75.0 (3.13)	86.0 (3.55)	77.3 (1.31)	72.1 (3.55)	<u>72.7 (5.25)</u>
SPA-SD-KGMM	<u>55.8 (4.02)</u>	71.9 (3.61)	81.4 (3.55)	<u>77.3 (4.73)</u>	81.4 (4.66)	81.8 (8.61)
Method	Pr2Cl	Pr2Ar	Pr2Rw	Rw2Ar	Rw2Cl	Rw2Pr
ADDA	37.7 (0.85)	50.2 (1.82)	58.5 (2.15)	61.9 (1.05)	42.5 (0.46)	70.7 (0.35)
AFN	47.9 (0.96)	58.6 (0.06)	77.0 (0.44)	69.3 (0.52)	52.9 (0.51)	80.0 (0.31)
BSP	39.5 (0.21)	52.9 (0.85)	72.3 (0.70)	64.9 (0.35)	48.8 (1.84)	76.5 (0.85)
CDAN	37.0 (1.08)	51.1 (0.35)	71.2 (0.15)	64.8 (0.30)	45.3 (0.57)	77.0 (0.35)
DAN	39.8 (0.49)	53.7 (0.68)	73.5 (0.30)	67.2 (1.34)	48.0 (1.07)	78.0 (0.57)
DANN	36.8 (0.78)	49.6 (0.80)	71.2 (2.94)	62.7 (0.14)	44.8 (0.78)	74.8 (0.14)
ERM	39.5 (0.28)	52.2 (0.49)	73.3 (0.17)	64.6 (0.07)	44.6 (0.10)	75.8 (0.21)
FDAL	39.6 (0.43)	58.3 (0.97)	75.1 (0.22)	67.4 (0.35)	46.3 (1.31)	78.9 (0.27)
JAN	41.3 (0.14)	56.1 (0.90)	74.1 (0.38)	67.0 (1.41)	48.8 (0.79)	77.0 (0.28)
MCC	36.4 (0.14)	52.3 (0.70)	71.8 (0.44)	64.4 (0.14)	44.8 (0.55)	76.7 (0.71)
MCD	37.7 (0.21)	52.9 (0.40)	73.1 (0.15)	66.2 (0.07)	45.5 (0.15)	77.1 (0.35)
MDD	38.1 (0.78)	52.2 (0.38)	71.4 (0.63)	64.0 (0.78)	46.0 (0.21)	76.0 (0.00)
SPA	58.1 (4.03)	65.6 (1.80)	83.7 (2.33)	71.9 (1.81)	55.8 (3.55)	81.8 (2.63)
SD-AGAU	46.0 (0.10)	63.7 (0.11)	78.2 (0.23)	72.8 (0.21)	51.4 (0.56)	81.0 (0.15)
SD-AGMM	46.2 (1.21)	64.2 (0.78)	77.6 (0.20)	72.9 (0.33)	52.8 (0.62)	81.4 (0.43)
SD-AVAE	47.1 (1.66)	66.1 (1.55)	78.8 (0.50)	<u>71.9 (0.16)</u>	49.2 (0.39)	80.6 (0.18)
SD-KGAU	45.7 (0.42)	63.5 (0.38)	68.7 (0.66)	72.8 (0.25)	47.4 (0.23)	79.9 (0.31)
SD-KGMM	45.4 (0.19)	65.3 (0.24)	78.9 (0.30)	63.0 (0.66)	52.2 (0.19)	80.7 (0.10)
SPA-SD-KGAU	55.8 (4.02)	68.8 (1.81)	83.7 (2.68)	75.0 (3.13)	<u>55.8 (3.55)</u>	93.2 (3.47)
SPA-SD-KGMM	<u>58.1 (3.55)</u>	81.2 (4.77)	72.1 (0.00)	71.9 (3.13)	51.2 (1.34)	<u>84.1 (3.47)</u>

Table 7: Accuracy and standard deviation on VisDA-2017 from sythetic domain to real domain, with 100%, 1% and 0.1% of target data available.

Method	100%	1%	0.1%
ADDA	68.3 (0.00)	68.3 (1.04)	63.3 (2.81)
BSP	<u>77.3 (1.25)</u>	71.0 (0.70)	66.1 (1.21)
CDAN	77.5 (0.96)	70.8 (0.81)	65.3 (1.14)
DAN	67.8 (0.46)	66.2 (0.10)	65.5 (0.81)
DANN	75.8 (0.40)	71.6 (0.44)	67.1 (1.73)
ERM	54.1 (0.46)	54.1 (0.45)	52.8 (0.74)
FDAL	72.2 (0.08)	70.2 (1.08)	70.7 (3.38)
JAN	69.0 (0.06)	68.3 (1.03)	63.4 (2.40)
MCC	72.8 (0.06)	72.5 (0.92)	63.8 (0.20)
MCD	75.1 (0.00)	69.4 (0.21)	63.2 (0.78)
MDD	77.2 (0.17)	69.3 (1.11)	64.3 (0.71)
SPA	74.2 (0.68)	78.0 (0.86)	<u>72.7 (1.05)</u>
SD-AGAU	68.3 (0.90)	66.7 (1.17)	69.2 (0.64)
SD-AGMM	67.2 (0.33)	66.7 (0.37)	68.6 (0.32)
SD-AVAE	67.6 (0.18)	68.2 (0.32)	67.8 (0.16)
SD-KGAU	64.8 (1.14)	69.6 (0.50)	68.7 (0.19)
SD-KGMM	64.9 (0.18)	65.3 (0.02)	66.8 (0.07)
SPA-SD-KGAU	71.1 (0.22)	<u>75.6 (1.20)</u>	74.5 (1.05)
SPA-SD-KGMM	69.8 (0.00)	<u>72.9 (0.38)</u>	<u>72.7 (1.05)</u>

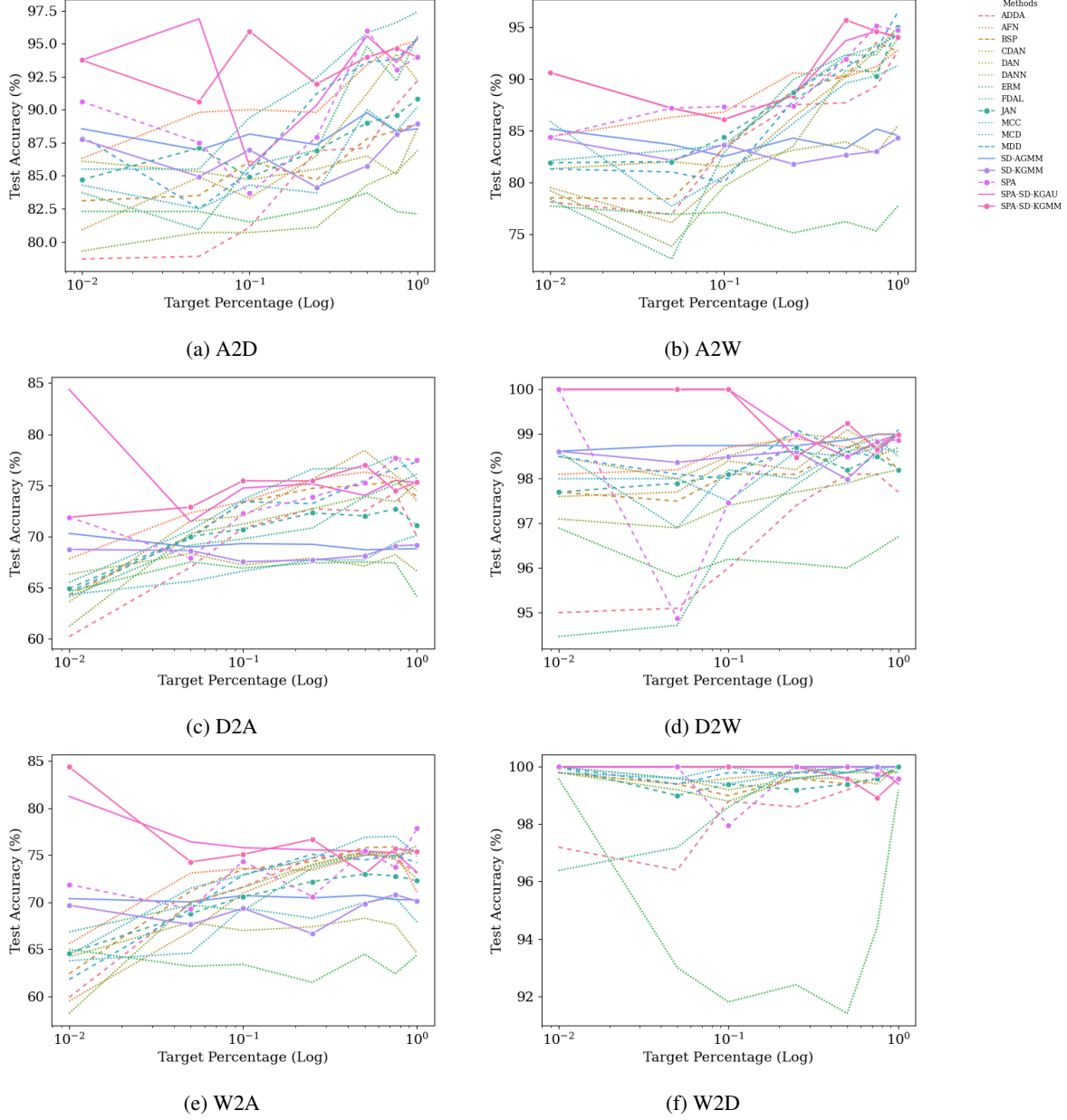


Figure 9: Comparison of UDA methods trained on varying percentages of target data, averaged across 6 domain pairs in Office31 dataset. Stein discrepancy-based methods (solid lines) have a smaller decline in accuracy at low levels of target data.

C Derivation of VAE Score Function

We present the detailed derivation of the score function of a VAE, which is one of the models used for the target distribution. A VAE is composed of an encoder \mathbf{E} , which maps inputs z to latent features ξ , and a decoder \mathbf{D} which maps from the latent space back to the input space. Let $p(z)$ be the data distribution. Let $p(z|\xi) = \mathbf{D}(\xi)$ represent the likelihood and $q(\xi|z) = \mathbf{E}(z)$ represent the approximate posterior. We estimate the score function $\nabla_z \log p(z)$ as follows:

$$\begin{aligned}
 \nabla_z \log p(z) &= \frac{1}{p(z)} \int \nabla_z p(z, \xi) d\xi \\
 &= \frac{1}{p(z)} \int \frac{\nabla_z p(z, \xi) q(\xi|z)}{q(\xi|z)} d\xi \\
 &= \mathbb{E}_{q(\xi|z)} \left[\frac{\nabla_z p(z|\xi) p(\xi)}{p(z) q(\xi|z)} \right] \\
 &\approx \mathbb{E}_{q(\xi|z)} \left[\frac{\nabla_z p(z|\xi) p(\xi)}{p(z) p(\xi|z)} \right] \\
 &= \mathbb{E}_{q(\xi|z)} [\nabla_z p(z|\xi) p(z|\xi)].
 \end{aligned} \tag{7}$$

Assuming $p(z|\xi)$ is a Gaussian distribution:

$$p(z|\xi) = \frac{1}{(2\pi)^{d/2}} \exp \left\{ -\frac{\|z - \mathbf{D}(\xi)\|^2}{2} \right\}, \tag{8}$$

where d is the dimension of the feature space. Combining (7) and (8) yields

$$\nabla_z \log p(z) = \left[\frac{1}{(2\pi)^{d/2}} \exp \left\{ -\frac{\|z - \mathbf{D}(\xi)\|^2}{2} \right\} \right]^2 (\mathbf{D}(\xi) - z),$$

where $\xi \sim \mathbf{E}(z)$.

D Algorithms

In this section, we present the algorithms used for Stein discrepancy based UDA. The main algorithm is presented in Section D.1. Since calculating Stein discrepancy requires an explicit score function for the target distribution, we also provide algorithms to compute the score function for the three target distributions we investigated, namely Gaussian, GMM, and VAE, in Section D.2.

D.1 Main Algorithm

In this section, we present the algorithm for Stein-discrepancy based domain adaptation. The kernelized version is presented in Algorithm 1, and the non-kernelized version is presented in Algorithm 2. Letting $z = g(x)$ be the features extracted from the input data x , the domain loss \mathcal{L}_D for the kernelized version is computed as in Equation 2 of the main paper:

$$\mathcal{L}_D = \mathbb{E}_{z_S} [\mathcal{A}_{\mathcal{D}_T} \mathcal{A}_{\mathcal{D}_T} k(z_S, z'_S)].$$

The domain loss \mathcal{L}_D for the non-kernelized version is computed as in Equation 1 of the main paper:

$$\mathcal{L}_D = \max_{f \in \mathcal{F}} \mathbb{E}_{z_S} [\mathcal{A}_{\mathcal{D}_T} f(z_S)].$$

Any standard classification loss, such as cross-entropy, can be used for \mathcal{L}_C .

D.2 Score Function

In this section, we present algorithms to calculate the score function for the three models used for the target distribution: Gaussian, GMM, and VAE. For simplicity of notation, the score functions are computed using the features $z = g(x)$. In the VAE algorithm, mean-squared error is a standard choice for the reconstruction loss \mathcal{L}_{VAE} , but other loss functions such as mean absolute error can also be used.

Algorithm 1 Kernelized Stein-Discrepancy Based Domain Adaptation

Input: Source and target training data $\mathcal{D}_S, \mathcal{D}_T$, feature extractor g with pre-trained parameters θ_g , classifier h with randomly initialized parameters θ_h , reproducing kernel k , learning rate η , trade-off parameter λ , epochs E , max iterations N

Output: Trained parameters $\theta = (\theta_g, \theta_h)$

for $n = 1$ **to** N **do**

 Sample batches (x_S, y_S) from \mathcal{D}_S and (x_T) from \mathcal{D}_T

 Compute classification loss $\mathcal{L}_C(\theta; h(g(x_S)), y_S)$

 Compute score function of \mathcal{D}_T from features $z_T = g(x_T)$

 Compute transfer loss $\mathcal{L}_D(\theta; x_S) = \mathbb{E}_{g(x_S)}[\mathcal{A}_{\mathcal{D}_T} \mathcal{A}_{\mathcal{D}_T} k(g(x_S), g(x'_S))]$

 Compute combined loss $\mathcal{L} = \mathcal{L}_C + \lambda \mathcal{L}_D$

 Compute gradients $\nabla_{\theta} \mathcal{L}$

 Update parameters $\theta \leftarrow \theta - \eta \nabla_{\theta} \mathcal{L}$

end for

Return: θ

Algorithm 2 Non-Kernelized Stein-Discrepancy Based Domain Adaptation

Input: Source and target training data $\mathcal{D}_S, \mathcal{D}_T$, feature extractor g with pre-trained parameters θ_g , classifier h with randomly initialized parameters θ_h , discriminator f with randomly initialized parameter θ_f , learning rate η , trade-off parameter λ , max iterations N

Output: Trained parameters $\theta = (\theta_g, \theta_h)$

for $n = 1$ **to** N **do**

 Sample batches (x_S, y_S) from \mathcal{D}_S and (x_T) from \mathcal{D}_T

 Compute classification loss $\mathcal{L}_C(\theta; h(g(x_S)), y_S)$

 Compute score function of \mathcal{D}_T from features $z_T = g(x_T)$

 Compute transfer loss $\mathcal{L}_D(\theta; x_S) = \mathbb{E}_{g(x_S)}[\mathcal{A}_{\mathcal{D}_T} f(g(x_S))]$

 Compute combined loss $\mathcal{L} = \mathcal{L}_C + \lambda \mathcal{L}_D$

 Compute gradients $\nabla_{\theta_f, \theta_g, \theta_h} \mathcal{L}$

 Update f parameters (maximization) $\theta_f \leftarrow \theta_f + \eta \nabla_{\theta_f} \mathcal{L}$

 Update g, h parameters (minimization) $(\theta_g, \theta_h) \leftarrow (\theta_g, \theta_h) - \eta \nabla_{(\theta_g, \theta_h)} \mathcal{L}$

end for

Return: $\theta = (\theta_g, \theta_h)$

Algorithm 3 Score Function for Gaussian Target Distribution

Input: Target features z_T

Output: Score function $\nabla \log \mathcal{D}_T$

Compute sample mean μ and covariance Σ of z_T

Return: $\nabla \log \mathcal{D}_T(z) = -\Sigma^{-1}(z - \mu)$

Algorithm 4 Score Function for Gaussian Mixture Target Distribution

Input: Target features z_T , number of components K , maximum iterations N

Output: Score function $\nabla \log \mathcal{D}_T$

Randomly initialize $\mu = \{\mu_k\}_{k=1}^K$, $\Sigma = \{\Sigma_k\}_{k=1}^K$, $\mathbf{w} = \{w_k\}_{k=1}^K$; ensure Σ_k is positive definite for all k

for $n = 1$ **to** N **do**

 Compute log probability $\mathcal{L}(\mu, \Sigma, \mathbf{w}; z_T)$

 Compute gradients $\nabla_{\mu, \Sigma, \mathbf{w}} \mathcal{L}$

 Update means $\mu \leftarrow \mu - \nabla_{\mu} \mathcal{L}$

 Update covariances $\Sigma \leftarrow \Sigma - \nabla_{\Sigma} \mathcal{L}$

 Update weights $\mathbf{w} \leftarrow \mathbf{w} - \nabla_{\mathbf{w}} \mathcal{L}$

end for

Return: $\nabla \log \mathcal{D}_T(z) = -\sum_{i=1}^K \gamma_i(z) \Sigma_i^{-1}(z - \mu_i)$, where $\gamma_i(z) = \frac{w_i \mathcal{N}(z | \mu_i, \Sigma_i)}{\sum_{j=1}^K w_j \mathcal{N}(z | \mu_j, \Sigma_j)}$

Algorithm 5 Score Function for VAE Target Distribution

Input: Target features z_T , VAE model composed of encoder \mathbf{E} and decoder \mathbf{D} , maximum iterations N

Output: Score function $\nabla \log \mathcal{D}_T$

Randomly initialize parameters θ_E, θ_D for \mathbf{E} and \mathbf{D}

for $n = 1$ **to** N **do**

 Compute latent features $\xi_T = \mathbf{E}(z_T)$

 Compute reconstruction loss $\mathcal{L}_{\text{VAE}}(\theta_E, \theta_D; z_T, \mathbf{D}(\xi_T))$

 Compute gradients $\nabla_{\theta_E, \theta_D} \mathcal{L}_{\text{VAE}}$

 Update encoder parameters $\theta_E \leftarrow \theta_E - \eta \nabla_{\theta_E} \mathcal{L}_{\text{VAE}}$

 Update decoder parameters $\theta_D \leftarrow \theta_D - \eta \nabla_{\theta_D} \mathcal{L}_{\text{VAE}}$

end for

Return: $\nabla \log \mathcal{D}_T(z) = \mathbb{E}_{q(\xi|z)}[\nabla_z p(z|\xi)p(z|\xi)]$

E Hyperparameters

We report the best hyperparameters for each of the Stein methods in the JAN framework on the VisDA-2017 dataset as a representative example of the hyperparameters in Tables 8-12. Stein discrepancy-based methods in the SPA framework were observed to be less sensitive to hyperparameters than in the JAN framework; for Gaussian target distribution, the kernel bandwidth was set to 10. For GMM target distribution, the bandwidth was set to 1. All other hyperparameters were left at the default from the original SPA implementation. For other methods, hyperparameters were selected using a randomized search algorithm, HyperOpt, and were optimized using RayTune, a machine learning and hyperparameter tuning library in Python. The ranges from which the hyperparameters were selected can be found in the code, available in the supplementary materials.

The trade-off parameter refers to the trade-off between the classification loss and the transfer loss. LR refers to learning rate and WD refers to weight decay. Cov. Eps. refers to covariance epsilon, which is used to regularize covariance matrices that become non-positive definite during training. Bottleneck refers to the dimension of the features; for methods where it is not reported it was left at the default value of 256. Bandwidth refers to the bandwidth of the kernel in kernelized methods; all experiments were conducted with a radial basis function (RBF) kernel. Adv LR, VAE LR, and GMM LR refer to the learning rates for the discriminator network f (in adversarial methods only), the VAE, and the GMM, for applicable methods.

Table 8: Best hyperparameters for kernelized method with Gaussian target distribution, on VisDA-2017 dataset.

Target %	Trade-Off	LR	Momentum	WD	Cov. Eps.	Label Smooth.	Bandwidth
100%	1.9363e-04	8.3729e-06	0.3935	4.2337e-04	9.9392e-04	0.7296	243.3
1%	3.0703e-08	1.4008e-04	0.3537	9.1421e-04	9.1609e-03	0.8325	284.3
0.1%	3.0703e-08	1.4008e-04	1.4008e-04	9.1421e-04	9.1609e-03	0.8325	284.3

Table 9: Best hyperparameters for adversarial method with Gaussian target distribution, on VisDA-2017 dataset.

Target %	Bottleneck Dim.	Trade-Off	LR	Momentum	WD	Cov. Eps.	Label Smooth.	Adv. LR
100%	128	1.37674e-06	1.70553e-09	0.2133	7.45643e-05	6.11751e-04	0.89012	6.00242e-04
1%	256	2.97230e-06	1.42854e-07	0.12044	8.47547e-04	5.54962e-02	0.89135	5.59339e-03
0.1%	128	4.0000e-06	1.1336e-08	0.3439	2.1000e-05	6.4811e-02	0.8625	5.1020e-03

Table 10: Best hyperparameters for kernelized method with GMM target distribution, on VisDA-2017 dataset.

Target %	Trade-Off	LR	Momentum	WD	Cov. Eps.	Label Smooth.	# GMM Comp.	Bandwidth	GMM LR
100%	1.0192e-08	4.2043e-07	0.1601	1.3923e-04	4.9397e-03	0.8917	16	187.2	6.8271e-03
1%	7.5309e-08	6.5494e-09	0.14	3.1455e-04	9.4000e-02	0.8746	8	176.5	1.0025e-02
0.1%	7.5309e-08	6.5494e-09	0.14	3.1455e-04	9.4000e-02	0.8746	8	176.5	1.0025e-02

Table 11: Best hyperparameters for adversarial method with GMM target distribution, on VisDA-2017 dataset.

Target %	LR	Momentum	WD	Cov. Eps.	Trade-Off	Label Smooth.	Bandwidth	# GMM Comp.	GMM LR	Adv. LR	Bottleneck Dim.
100 %	4.0945e-07	0.1795	2.6394e-05	1.2426e-04	4.5856e-05	0.8903	148.6	8.0	2.8751e-03	1.2373e-04	128.0
1%	3.7920e-06	0.1127	1.1177e-04	9.4443e-02	1.1148e-04	0.8753	29.81	24.0	6.6891e-05	3.2996e-02	128.0
0.1%	3.7920e-06	0.1127	1.1177e-04	9.4443e-02	1.1148e-04	0.8753	29.81	24.0	6.6891e-05	3.2996e-02	128.0

Table 12: Best hyperparameters for kernelized method with VAE target distribution, on VisDA-2017 dataset.

Target %	LR	Bottleneck Dim.	Trade-Off	Label Smooth.	Hidden Dim.	Latent Dim.	VAE Steps	Adv LR	VAE LR	Momentum	WD
100%	1.3096e-07	128.0	0.9636	0.89	16.0	16.0	4.0	1.2071e-03	5.9582e-04	0.311	2.8761e-04
1%	1.9645e-06	128.0	1.8354e-07	0.8927	128.0	5.1200e+02	1.0	6.0997e-03	1.2185e-04	0.1708	4.4748e-04
0.1%	1.9645e-06	128.0	1.8354e-07	0.8927	128.0	5.1200e+02	1.0	6.0997e-03	1.2185e-04	0.1708	4.4748e-04